

**INTERFACIAL ADHESION IN
POLYMER LAMINATED SHEET METALS**

**ASSESSMENT OF INTERFACIAL ADHESION IN
POLYMER LAMINATED SHEET METALS**

By

HADI NOORI, M.A.Sc., B.Sc.

A Thesis

Submitted to the School of Graduate Studies

in Partial Fulfilment of the Requirements

for the Degree of Doctor of Philosophy

McMaster University

©Copyright by Hadi Noori, August 2015

McMaster University DOCTORATE OF PHILOSOPHY (2015) Hamilton, Ontario
(Mechanical Engineering)

TITLE: Assessment of Interfacial Adhesion in Polymer Laminated Sheet Metals

AUTHOR: Hadi Noori
B.Sc. (Ferdowsi University of Mashhad)
M.A.Sc. (University of Tehran)

SUPERVISOR: Dr. Mukesh JAIN

NUMBER OF PAGES: xiv, 77

LAY ABSTRACT

The polymer laminated sheet metal (PLSM) is a layered material which involves a sheet metal substrate, a thin polymer film and an adhesive layer between the film and the substrate. In this thesis, the main focus has been devoted to characterizing and improving the adhesion properties of the PLSM system for forming applications.

A new experimental methodology has been devised for analyzing the effects of deformation-induced surface roughness of metallic substrate and deformation-induced residual stress in polymer adherends on interfacial peel properties of PLSMs.

A novel interpretation of the results obtained from rate-independent cohesive zone modeling of peel test has revealed the significance of peel speed in determining the interface strength between the adhesive and the metallic substrate.

In another part of this thesis, the effects of two substrate surface alteration techniques, grinding and knurling, on peel properties of PLSMs have been studied.

ABSTRACT

The polymer laminated sheet metal (PLSM) is a layered material which involves a sheet metal substrate, a thin polymer film and an adhesive layer between the film and the substrate. The adhesion properties between the bonded materials are among the most important issues in PLSM forming operations. In this thesis, the main focus has been devoted to characterizing and improving the adhesion properties of the PLSM system for forming applications.

Metallic surface roughness evolution and residual stress development in polymer adherends are two consequences of the plastic deformation of the PLSMs. In chapter 2, the effect of these factors on interfacial adhesion strength between metallic substrate and polymer adherend (polymer film with a thin uniform pressure-sensitive adhesive layer on one side) is investigated by devising a new experimental methodology. This methodology is based on two different protocols for preparation of peel sample, one involving pre-straining in uniaxial tension of the metallic substrate prior to lamination and the other involving post-lamination pre-straining of the PLSM.

In chapter 3, the peel test results of two different types of PLSMs at different peel speeds are analyzed with two different approaches common in cohesive zone modeling in the literature, namely linear elastic stiffness approach and critical maximum stress approach. The modeling results revealed the significance of the peel speed in determining the interface strength between the adhesive and metallic substrate.

In chapter 4, two mechanical treatment techniques of grinding and knurling are implemented to alter the metallic substrate surface roughness before lamination. Peel strength of these samples are investigated at different peel speeds and at different peel loading directions with respect to the grinding and knurling directions.

ACKNOWLEDGEMENTS

I would like to gratefully thank my supervisor, Professor Mukesh Jain, for providing me the opportunity to be part of his research team. Under his supervision, I have learned and practiced the professionalism in academic environment. The invaluable lessons that I have learned during research work with him can be used in other aspects of my life.

Special thanks to Dr. Peidong Wu, Dr. Gregory Wohl and Dr. Michael Tait for their professional recommendations and technical advices which have been very helpful to overcome many difficulties during my research studies at McMaster University.

I have also received technical assistances from technicians at machine shop at Department of Mechanical Engineering, microscopy laboratories at Department of Materials Science and Engineering and advanced machining laboratory at Department of Mechanical Engineering. I would like to thank them all because this work was not possible without their help.

The financial support of 3M Canada Corporation, Ontario Centre of Excellence (OCE) and Natural Sciences and Engineering Research Council of Canada (NSERC) for part of my studies at McMaster University is gratefully appreciated. Also, I would like to thank Dr. Michael Thompson and his research team at Department of Chemical Engineering who provided me access to the laboratories for conducting a majority of the experiments for this study.

All the inspiration that I have gained, all the efforts that I have devoted, and all the patience that I have endured during my PhD studies are dedicated to my dear wife, Maryam, and my lovely daughter, Mandana.

Table of Contents

Descriptive Note	ii
LAY ABSTRACT	iii
ABSTRACT	iv
ACKNOWLEDGEMENTS	v
Table of Contents	vi
List of Figures	viii
List of Tables	x
List of Abbreviations and Symbols	xi
Declaration of Academic Achievement	xiv
Chapter 1. General introduction	1
1.1 Background	1
1.2 Adhesion measurement in PLSMs (peel test)	2
1.2.1 Numerical analysis of peel test	5
1.3 Effect of deformation on interfacial adhesion in PLSMs	7
1.3.1 Effect of residual stress on interfacial adhesion in PLSMs	8
1.3.2 Effect of surface roughness on interfacial adhesion in PLSMs	8
1.3.2.1 Effect of pre-existed surface roughness of metallic substrate	9
1.3.2.2 Effect of deformation-induced surface roughness of metallic substrate	10
Chapter 2. Effect of deformation-induced residual stress on peel strength of polymer laminated sheet metal	11
2.1 Introduction	12
2.2 Experimental procedure	15
2.2.1 Laminate constituent materials.	15
2.2.2 Protocols for peel test sample preparation	16

2.2.3	180° peel tests	19
2.2.4	Uniaxial tensile testing of adherends	21
2.3	Results and discussion	22
2.3.1	Effect of adherend type on peel strength	23
2.3.2	Effect of surface roughness on peel strength	23
2.3.3	Effect of uniaxial deformation on peel strength	24
2.3.4	Effect of peel speed on peel strength	28
2.4	Conclusions	31
2.5	Acknowledgements	32
Chapter 3.	Significance of Peel Test Speed on Interface Strength in Cohesive Zone Modeling	33
3.1	Introduction	33
3.2	Experimental procedure	36
3.2.1	Materials and peel sample preparation	36
3.2.2	Peel test	37
3.2.3	Uniaxial tensile test	37
3.3	Cohesive zone modeling of peel test	39
3.4	Results and discussion	43
3.4.1	Linear elastic stiffness approach	43
3.4.2	Critical maximum stress approach	44
3.4.2.1	Case I: Adherend B as a reference	45

3.4.2.2	Case II: Adherend C as a reference	46
3.5	Conclusions	49
3.6	Appendix A	50
Chapter 4.	Influence of metallic substrate surface engineering on peel resistance of adhesively bonded polymer film	51
4.1	Introduction	51
4.2	Experimental procedure	54
4.2.1	Materials and peel test sample preparation	54
4.2.1.1	Grinding	56
4.2.1.2	Rolling the sheet metals with a redesigned knurling tool	57
4.2.2	Peel test	57
4.3	Results and discussion	60
4.4	Conclusions	64
4.5	Acknowledgement	65
Chapter 5.	Discussions	66
Chapter 6.	General conclusions	70
	Recommendations for future work	72
	Bibliography	73

List of Figures

Figure 1.1	The schematic of some peel test techniques (a) Basic peel test (b) Roller-assisted peeling (c) Floating-roller test and (d) Climbing-drum test [Kawashita et al., 2005]	3
Figure 1.2	Peel force-deflection (displacement) trace: the ideal case (a) and an experimental example (b) [Moore and Williams, 2001]	4
Figure 1.3	A triangular form of the traction-separation relationship for the cohesive zone at the peel front	6

Figure 2.1 The 180° peel test configuration (a), a schematic of a peel sample (b), through-thickness geometry of the PLSM (c) and de-bonded surfaces of the sheet metal and polymer adherend B after 180° peel test (d)	17
Figure 2.2 Surface roughness of metallic substrate (AISI 430) versus uniaxial tensile pre-strain value	18
Figure 2.3 Flowchart representing the sequences for preparation and peel testing of PAL and PBL samples	19
Figure 2.4 Nominal uniaxial tensile stress-strain curves for polymer adherends obtained at three different cross head speeds. The curves for 10 mm/min are from reference.	21
Figure 2.5 Normalized peel force versus pre-strain values for PBL and PAL samples at 10, 50 and 250 mm/min peel speeds	26
Figure 2.6 Delamination of the Adherend B from the edges of the PAL samples after pre-straining to the value of 0.07. The dents on the polymer surface at left hand side were caused by the tensile machine grips. The sheet metal substrate is hidden under the black polymer adherend	27
Figure 2.7 Difference of $(F/b)_{PBL} - (F/b)_{PAL}$ at different peel speeds	29
Figure 2.8 Microscopic views of the polymer surface showing the effect of peel speed on the peel arm of adherend B with no pre-strain. The far right image is a SEM micrograph and the rest are optical micrographs	30
Figure 3.1 A triangular form of the traction-separation relationship for the cohesive zone at the peel front	33
Figure 3.2 Nominal stress-strain curve for two adherend materials at 10 mm/min cross-head speed. The symbol e^* represents the nominal strain at which the nominal stress drops for adherend B due to the rupture of the PET coat on its top surface	37
Figure 3.3 The schematic of the 180° peel test. The parameter R is the radius of curvature at root rotation and δ is the characteristic length	40

Figure 3.4 Microscopic views of the polymer surface showing the effect of peel speed on the peel arm of adherend B. The top right picture is the SEM micrograph and the rest are obtained by the optical microscope	46
Figure 3.5 Yield strength and interface strength of adherend B with respect to the peel speed (a) and (b) fitted curve by using the least square method showing the relationship between interface strength, yield strength and peel speed based on equation (3.4.2.2.1)	47
Figure 4.1 A schematic of the PLSM strip	53
Figure 4.2 Images of the ground surface, (a) stereoscopic image from optical microscope, (b) 3D image from Zygo optical surface profiler	56
Figure 4.3 Images of the knurled surface, (a) stereoscopic image from optical microscope (bright annealed surface is visible in areas adjacent to the dark groove region), (b) 3D image from Zygo optical surface profiler	57
Figure 4.4 A typical peel force versus displacement trace from experiment showing steady-state peel zone	57
Figure 4.5 Normalized steady-state peel force of adherends HGF and LGF from ground and bright-annealed surfaces at two peel speeds	58
Figure 4.6 Scanning electron micrograph shows the through-thickness interface of the adhesive and SSSS, the latter with an average roughness value of 0.65 μm	59
Figure 4.7 Stereoscopic images of top surface of adherend HGF before and after peeling at 50 and 250 mm/min peel speeds	60
Figure 4.8 Normalized steady-state peel force of adherends HGF and LGF from knurled and bright-annealed surfaces at two peel speeds	61

List of Tables

Table 2.1 3M TM adherend materials	15
Table 2.2 The summary of peel tests variables	20

Table 2.3 Mechanical properties of the peel arm at different uniaxial tensile test speeds	21
Table 2.4 The constants H and m of power law equation for the fitted curves in Figure 2.7	30
Table 3.1 3M polymer films and adhesives	36
Table 3.2 Mechanical properties of the peel arm at different uniaxial tensile test speeds	38
Table 3.3 Analytical results for both adherends based on linear-elastic stiffness approach	43
Table 3.4 Analytical results for adherend C based on critical maximum stress approach (case I)	44
Table 3.5 Analytical results for adherend B based on critical maximum stress approach (case II)	45
Table 4.1 3M polymer films and adhesives	53
Table 4.2 Decrease in peel resistance of adherends from knurled surface compared with bright-annealed surface at two peel speeds	62

List of Abbreviations and Symbols

CZM = cohesive zone model

IAS = interfacial adhesion strength

IPS = interfacial peel strength

PAL = pre-straining after lamination

PBL = pre-straining before lamination

PDMS = polydimethylsiloxane

PE = polyethylene

PET = polyethylene terephthalate

PLSM = polymer laminated sheet metal

PP = polypropylene

PSA = pressure sensitive adhesive

PVC = polyvinyl chloride

RIMIBM = reactive ion assisted interface bonding and mixing

SSSS = stainless steel sheet substrate

XPS = X-ray photoelectron spectroscopy

b = peel arm width

E = elastic modulus of peel arm

E_a = elastic modulus of adhesive

E_f = elastic modulus of polymer film

E_2 = transverse elastic modulus of peel arm

e = nominal pre-strain value

F = peel force

F_a = force carried by adhesive

F_f = force carried by polymer film

F_t = total force applied on adherend

G = total peeling energy

G_c = adhesion fracture energy

G_d = plastic deformation of peel arm

G_e = elastic energy release rate

G_t = total peeling energy including elastic energy release rate

H = constant of power law equation for the fitted curves in Figure 2.7 and also ratio of film thickness to adhesive thickness

h = thickness of peel arm

h_a = thickness of adhesive

h_f = thickness of polymer film

k_0 = a parameter that corresponds to the stage at which the peel arm exhibits the minimum radius of curvature at the end of the bending process of the peel arm

k_s = stiffness of the peeling material

m = constant of power law equation for the fitted curves in Figure 2.7

M_p = fully plastic moment

N = number of layers of adherend

R = radius of curvature at root rotation

u = extent of separation in cohesive zone at peel front

V_{ref} = reference peel speed

δ = characteristic length

ε_y = yield strain of peel arm

θ = peel angle

θ_0 = root rotation in cohesive zone

ρ = ratio of polymer film elastic modulus to adhesive elastic modulus

σ = traction in cohesive zone at peel front

σ_{max} = interface strength

σ_y = initial yield strength of peel arm

Declaration of Academic Achievement

This thesis is based on the following publications:

Chapter 2. H. Noori, M. Jain, K. Nielsen, and F. Brandys, Effect of deformation-induced residual stress on peel strength of polymer laminated sheet metal, accepted for publication in the Journal of Adhesion, May 2015, DOI: 10.1080/00218464.2015.1050718.

Chapter 3. H. Noori, M. Jain, K. Nielsen, and F. Brandys, Significance of peel test speed on interface strength in cohesive zone modeling, accepted for publication in the Journal of Adhesion, November 2014, DOI: 10.1080/00218464.2014.993755.

Chapter 4. H. Noori, M. Jain, K. Nielsen, and F. Brandys, Influence of metallic substrate surface engineering on peel resistance of adhesively bonded polymer film, published in the Journal of Adhesion Science and Technology, vol. 29, pp. 1403-1413, 2015.

Author's contribution to publications:

All of the above journal papers were written by the author and his co-workers. The following are the contributions by author in these publications:

- (a) Devising and conducting the experiments
- (b) Analyzing and preparing the results
- (c) Preparing the manuscript

Chapter 1. General introduction

1.1 Background

Among the recent materials used for automotive sheet forming processes, the bonded sheets have been considered as an attractive alternative. Different physical and mechanical properties of materials involved in the bonded sheets provide a combination of benefits and improve the in-service performance. Polymer laminated sheet metals (PLSMs) are a new class of bonded sheet materials which have been made by adhering a polymer film to the metallic sheet surface by using an adhesive layer for various applications. Good strength and formability of the bare metallic sheet combined with unique physical and mechanical properties of the polymers such as corrosion resistivity, lubricity and elimination of the post forming painting and finishing potentially offer these materials certain advantages over bare base metallic sheets. It is apparent that by reducing or eliminating the post-process finishing, the production would be more cost effective. In addition, reducing the process steps and therefore reducing the volatile organic compound emissions during manufacturing, make the operations more environmentally friendly. Using various kinds of plastic films and metallic sheets may provide a wide range of applications which are of interest in different industries such as automotive, food, decoration, aerospace, etc.

Adhesion between the materials involved in the PLSM is one of the most important factors affecting the applicability of this new material. The topic of adhesion includes four main fields of study including (1) formation of adhesion, (2) characterization of the interfaces between the adhered materials, (3) delamination of the interfaces and (4) failure analysis of interfaces [Marshall et al., 2010]. Due to the type of the adhered materials and the application of the built structure, the approach in studying these four areas would be different. The mechanisms of adhesion discussed in the literature have been classified to six main categories including electrostatic, weak

boundary layers, physical adsorption, diffusion, chemical and mechanical interlocking [Comyn, 1997; Schultz and Nardin, 1999]. Physical adsorption theory always contributes in adhesion mechanism because all of the adhesive bonds involve molecules in intimate contact [Comyn, 1997]. Rather than physical adsorption mechanism, for the studied PLSMs in this thesis, the mechanical and chemical interlocking mechanisms were the adhesion mechanisms between materials involved in the PLSMs' structures. The adhesion between the adhesive and sheet metal was based on mechanical interlocking and the mechanism of adhesion between polymer film and adhesive was chemical interlocking.

1.2 Adhesion measurement in PLSMs (peel test)

Investigation of the adhesion characteristics requires conducting suitable mechanical tests to assess the performance of the PLSMs. One of the most common tests for measuring the adhesion properties for the structures with the flexible laminates or coatings is the peel test [Lacombe, 2005]. Figure 1.1 shows the schematics of some of the peel test methods. By the use of the peel test, the reaction force and de-bonding length of the adherend from the substrate is measured. Figure 1.2 (a) illustrates the force-deflection (displacement) data for ideal peel test. In this figure, the force will be increased linearly at the first stage of the curve. This stage is attributed to the elastic energy stored in the adherend material as well as the initiation of adherend delamination from the substrate. The second stage is the plateau line which represents the crack propagation during peeling. The idealized peel test results assume the uniform adhesion at the interface and no plastic deformation of the materials involved in the structure. Therefore, the level of the plateau line can be easily considered as the adhesion strength. Since none of the above assumptions will be satisfied during the real peel test, the force-displacement results show usually a difference compared to the ideal results. Figure 1.2 (b) shows a typical peel test data obtained from peeling the polyethylene from the structure composed of polyethylene, aluminum and paper [Moore and Williams, 2001]. This figure shows a

linear curve at the early stage of peeling similar to the ideal results. However, the second stage is much fluctuated and includes the peaks and valleys. The high level of the curve has been interpreted as the cohesive fracture in the peel arm (adherend) and the low level has been interpreted as an adhesive fracture between the peel arm and the substrate [Moore and Williams, 2001]. From delamination point of view, there are two mechanisms proposed for peeling the adherend from the substrate: de-adhesion and de-cohesion. Adhesion involves molecular interaction at the interface between the materials while cohesion involves intermolecular attractions between like molecules/atoms [Marshall et al., 2010]. Analysis of the adhesion strength would be more accurate if the delamination mechanism and geometry is known during peeling.

Moore [2008] has reviewed the peel test protocols and experimental activities performed via this test. The effects of peel angle, speed of peeling, peel arm thickness, type of the peel test method, etc. on the adhesion strength have been investigated experimentally. Analysis of the peel test results is strongly dependent to the test conditions and the deformation behavior of peeling materials. When the required peeling force is more than the materials resistance force for plastic deformation or fracture, analyzing of the peel test results must take into account the post-elastic behavior of the materials in addition to their elastic deformation [Kinloch and Williams, 2002]. In this case, the energy required for de-bonding initiation and propagation is contributed not only by the de-adhesion strength between the materials, but also by the energy dissipation in the adhered materials.

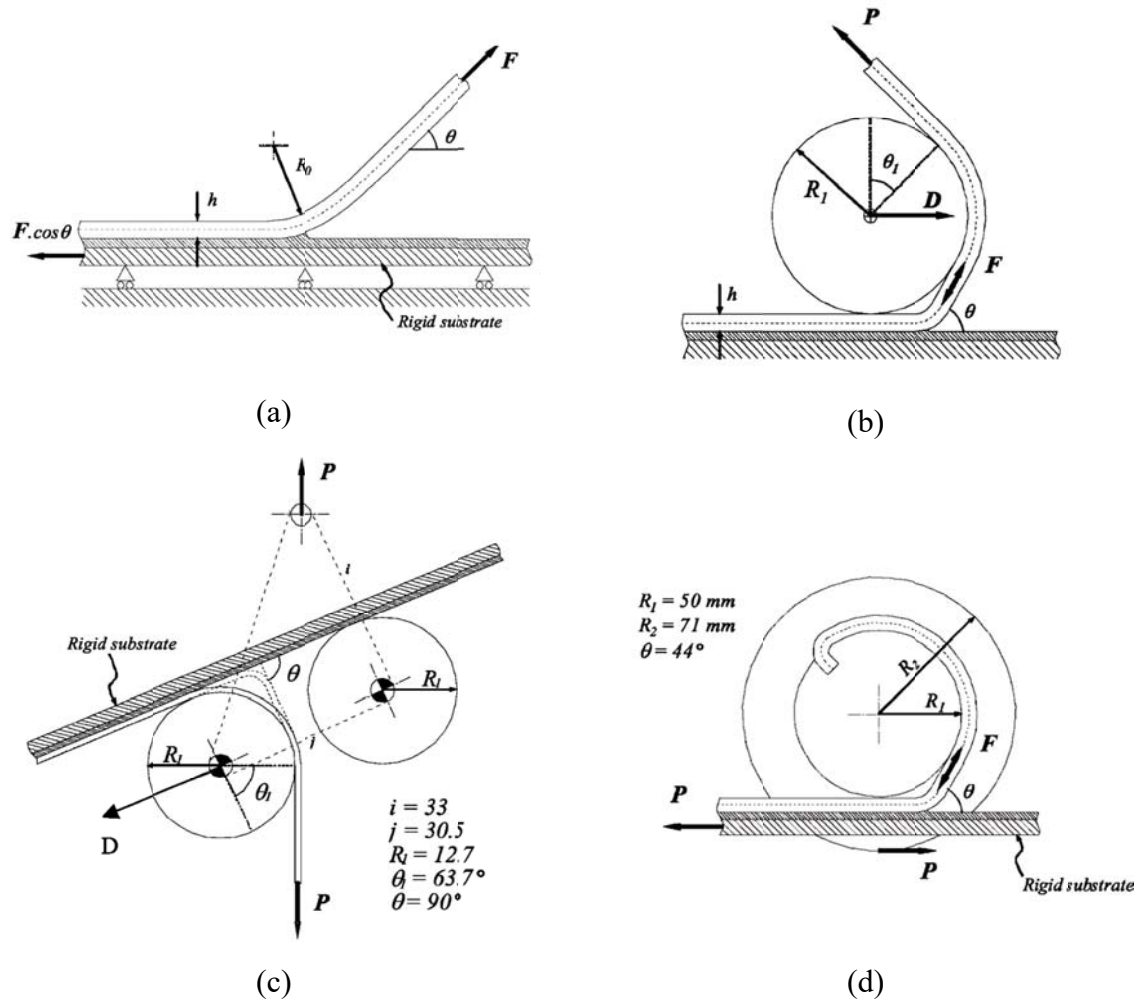


Figure 1.1 The schematic of some peel test techniques (a) Basic peel test (b) Roller-assisted peeling (c) Floating-roller test and (d) Climbing-drum test [Kawashita et al., 2005].

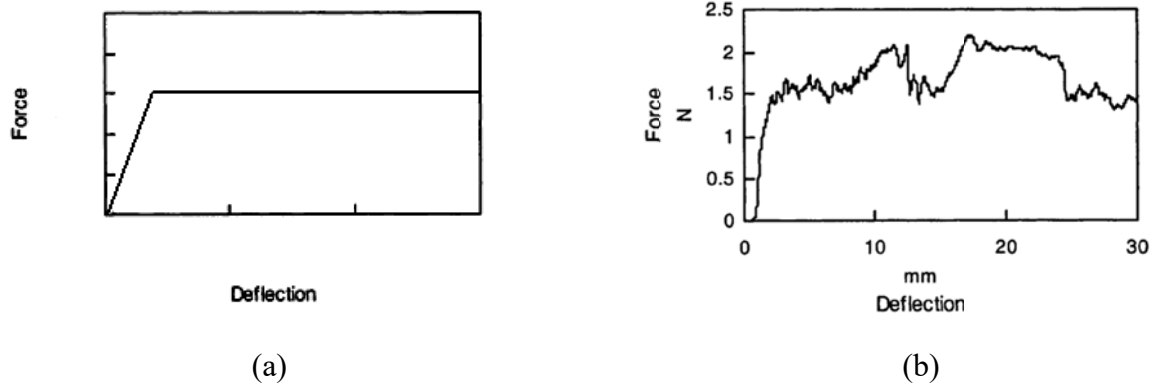


Figure 1.2 Peel force-deflection (displacement) trace: the ideal case (a) and an experimental example (b) [Moore and Williams, 2001].

1.2.1 Numerical analysis of peel test

For numerical analysis of the peel test results, three main approaches have been developed including stress based models, fracture mechanics models, and cohesive zone models (CZMs). Stress based approach deals with the stress and strain determination of the adherend and substrate during peeling. Some numerical issues due to the stress singularities at the tip of the crack have been reported [Kim and Aravas, 1988]. However, it has been employed for predicting the onset of damage (crack initiation) in bonded materials. In fracture mechanics approach, the balance of energy is considered for the process. By this technique, the applied energy on the system for peeling the adherend from the substrate is related to the dissipated energy by the interfacial debonding and the stored energy in the adherend and substrate during peeling [Kim and Kim, 1988; Thouless and Jensen, 1992; Kinloch et al., 1994]. Numerical analysis by the use of these techniques needs the initial crack (damage) to be well defined. This method has been utilized for predicting the propagation of the damage (crack) between the bonded material elements in composite-type structures. More recently, some of the disadvantages of above models have been overcome by developing the so-called cohesive

zone models. This approach is capable of simulating both damage initiation and propagation in the adhesively joined materials [Wei and Hutchinson, 1998; Georgiou et al., 2003].

The CZM is based on a traction-separation (σ - u) relationship which is assumed to characterize the separation of the interface at the peel front. The traction-separation relationship is defined by two primary parameters which are the adhesion fracture energy (G_c) and the interface strength (σ_{max}). Figure 1.3, for example, shows a triangular form of the traction-separation relationship for the cohesive zone at the peel front. The σ_{max} is assumed to be a critical maximum stress in the damage zone ahead of the crack, k_s is the stiffness of the peeling material and b is the width of the peel arm. Although it has been shown that G_c , as obtained by CZM, is fairly insensitive to the form of the traction-separation relationship [Williams and Hadavinia, 2002], it is strongly dependent on the interface strength [Wei and Hutchinson, 1998]. Therefore, it is unlikely that an accurate estimation of adhesion fracture energy from peel test data can be made without prior information about interface strength. This topic will be discussed in more detail in Chapter 3.

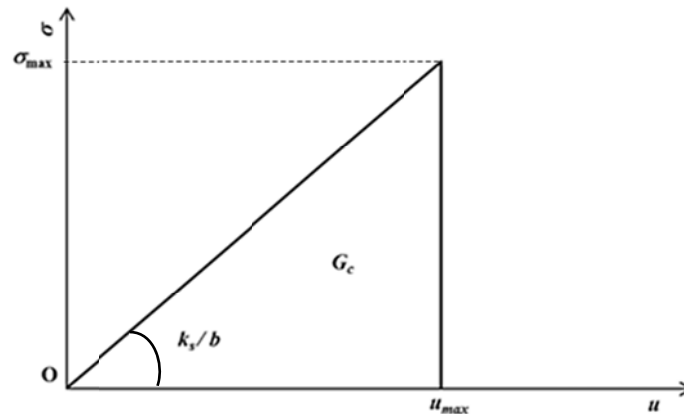


Figure 1.3 A triangular form of the traction-separation relationship for the cohesive zone at the peel front.

1.3 Effect of deformation on interfacial adhesion in PLSMs

Deformation of the PLSMs may deteriorate interfacial adhesion, thereby limiting their use in the as-formed state [Huang and Wang, 2013; Vayeda and Wang, 2007; Takiguchi and Yoshida, 2003; van den Bosch et al., 2008]. The differences in deformation behavior of the constituents (sheet metal, adhesive and polymer film) in PLSM structure is the primary reason for loss of adhesion.

Deformation of the PLSM results in two simultaneous consequences: first, the residual stresses development in polymer adherend¹ and second, the surface roughness evolution of metallic substrate. They could either benefit or harm the interfacial adhesion depending on how they act toward enhancing or deteriorating the bonding between the involved materials. In an ideal case, the energy stored in the adherend material due to the tensile residual stress should be less than the interfacial adhesion energy due to the contact between the bonded materials; thereby the adherend materials do not delaminate after deformation. Increasing the area of contact between bonded materials is beneficial to interfacial adhesion [Chiche et al., 2000; van Tijum et al., 2007]. On the other hand, increasing the tensile residual stresses promotes interfacial delamination [Vellinga et al., 2008].

The energy due to the imposed stresses is stored or dissipated through change in the microscopic features in the bulk of the polymer adherend [Aklonis and MacKnight, 1983] (e.g., molecular arrangement in polymer, molecular chain elongation, etc.) while the substrate surface roughness changes the interfacial adhesion energy between the contacting materials (sheet metal and adhesive).

¹ Polymer adherend as a term refers to the combination of polymer film and adhesive layer.

1.3.1 Effect of residual stress on interfacial adhesion in PLSMs

The adhesion properties in the PLSM structure may be strongly influenced by the residual stresses in the adherend material caused by lamination technique or forming operations. He et al., [1994] showed the important role of the residual stress in delamination of the thin film from the substrate by analyzing the energy release rate of the interfacial and penetrating cracks in bonded materials. Krishna [1996] employed the critical energy release rate criterion to predict the de-bonding of polyimide film bonded to glass (elastic substrate) in the presence of residual stresses caused by coating technique. Clyne and Gill [1996] reviewed the experimental and numerical research studies about the residual stress effect on interfacial adhesion in thermal spray coatings. They showed the effectiveness of the concept of energy release rate in evaluation and prediction of the interfacial de-bonding. Yu and Hutchinson [2003] explored the partial and full delamination of the thin film which was under tensile residual stress. They revealed the dependence of delamination to the geometry and mismatch in elastic properties of the bonded thin film and substrate. In all of the above work, the mismatch between the thermal expansions of the bonded materials was considered as a source of the residual stress. Deformation of the bonded materials such as PLSMs can induce the residual stress which consequently limits the application of these materials. In Chapter 2, an experimental methodology will be presented for assessment of the effect of deformation-induced residual stress on interfacial adhesion in studied PLSMs.

1.3.2 Effect of surface roughness on interfacial adhesion in PLSMs

Since the adhesion mechanism between the adhesive and sheet metal substrate in studied PLSMs was mainly the mechanical interlocking mechanism, the surface roughness of the metallic substrate on adhesion properties plays an important role. The metallic surface roughness may get altered either before lamination or after lamination when the PLSM is under deformation process. The latter is due to the fact that the metallic surface roughens

during mechanical loading and is caused by the dislocation activities. More details about the effect of surface roughness on adhesion properties between bonded materials will be reviewed in following sections.

1.3.2.1 Effect of pre-existed surface roughness of metallic substrate

Surface treatment of the adhered materials before adhesion is one of the known methods for enhancing the adhesion strength. The researchers mostly focused on the use of chemical surface treatment techniques such as etching, conversion coatings, etc. to promote the adhesion properties especially between the metals and polymers [Carre and Schultz, 1983; Ranucci et al., 2001; Lee and Qu, 2003; Ge et al., 2003]. For example, Fabrin et al., [2007] used the injection molding technique for adhering the thermoplastic elastomer to a pure aluminum sheet. The surface of the aluminum sheet was etched with different etching regimes and they investigated the effect of different surface treatment by evaluation of the adhesion strength with 180° peel test. In their work, the peel test data showed a much fluctuated patterns which resulted in a quite large standard deviation in determination of the adhesion strengths. They did not try to analyze the peel test results by considering the plastic deformation of the adherend materials. As another attempt for surface treatment, Müller et al. [1994] have modified the titanium surface with a laser to improve the shear loading capacity of the PMMA polymer adherend. Also, some researchers have studied the effect of mechanical treatment techniques on the adhesion properties between steels and adhesives. For example, Watts and Castle [1984] have compared the efficiency of four techniques including grit blasting, abrasion, polishing and chemical etching for surface treatment on mild steel to bond to the epoxy. They reported that the rate of the de-bonding in cathodic debondment test is least for grit-blasted surface compared to the other treated surfaces. However, the contamination of the surface caused by grit blasting may affect the durability of the improved adhesion properties. Wu and Lu [1997] have improved the adhesion between the sputter deposited aluminum and Teflon by treating the interface with reactive ion assisted interface

bonding and mixing (RIMIBM) technique. They have supported their claim with the peel and XPS (X-ray Photoelectron Spectroscopy) testing techniques. Kim et al. [2005] have improved dramatically the adhesion strength between Cu/Cr film and Polyimide substrate by roughening the polymer surface with inductively coupled oxygen plasma technique. They have employed the T-peel test as an evaluation method for measuring the adhesion properties. A very little is known about the relationship between the surface treatment of the stainless steels which have a chromium oxide layer on their surfaces and the adhesion properties with the PSAs. This topic will be dealt with in Chapters 2 and 4.

1.3.2.2 Effect of deformation-induced surface roughness of metallic substrate

Surface roughening of the metallic substrate in PLSMs during large plastic deformations may influence the interfacial adhesion properties between polymer films and substrate. Numerical study on uniaxial plane strain tension of polymer coated sheet metals showed that local delamination during deformation led to a decrease in contact area. However, metallic surface roughening increased the contact area and competed with the effect of local delamination on adhesion loss [van Tijum et al., 2007]. In another study [van den Bosch et al., 2008], although it was shown that deformation of the polymer coated steel decreased the peel strength of the polymer coat, the effect of deformation-induced surface roughness of metallic substrate was not analyzed independently on adhesion properties. Experimental analysis of the effect of deformation-induced surface roughness, independently from other factors which influences the adhesion properties of the PLSMs, is a major obstacle due to the technical difficulties. Regarding this issue, an experimental methodology will be proposed in Chapter 2.

Chapter 2. Effect of deformation-induced residual stress on peel strength of polymer laminated sheet metal

Abstract — The adhesion between adhesively bonded polymer film and a metallic sheet substrate in a polymer laminated sheet metal (PLSM) subjected to large deformation, such as in a forming process, is influenced by two deformation-induced factors. These are (i) evolution of surface roughness of metallic substrate with applied strain and (ii) development of residual stress in the polymer adherend (polymer film with a thin uniform adhesive layer on one side) arising from significant differences in the deformation behavior of metal and polymeric components. A new experimental methodology was devised in this study to decouple the effects of substrate surface roughness and residual stress on interfacial peel strength (IPS) of uniaxially deformed PLSMs. This methodology was based on 180° peel testing of PLSM specimens prepared under two different lamination conditions, one involving systematic pre-straining in uniaxial tension of the metallic substrate prior to lamination and the other involving post-lamination pre-straining of the PLSM. The role of pre-strain and peel test speed, for the above laminations conditions, were critically analyzed for their effect on IPS of two differently tailored PLSM systems. The IPS results were attributed to the effect of deformation-induced residual stress and metallic surface roughness. The analysis suggests that IPS is strongly dependent upon the residual stress induced by uniaxial deformation but only marginally on substrate surface roughness depending upon the constituents (film and adhesive) of the adherend. The magnitude of pre-strain was inversely and non-linearly related to IPS for both deformed PLSMs. Peel test speed, on the other hand, showed a more complex behavior in terms of IPS for the two PLSM systems.

Keywords: polymer laminated sheet metal, uniaxial deformation, residual stress, surface roughness, peel test

2.1 Introduction

Polymer laminated sheet metals (PLSMs) are a new class of materials that offer certain advantages over bare metallic sheets for forming applications. The primary advantages are in terms of finished components where the outer film surface offers corrosion protection and appealing surface appearance. These systems are possibly less costly and more environment friendly compared to their formed and subsequently painted wholly metallic counterparts. PLSMs are typically prepared by adhering a thin polymer film to the metallic sheet substrate by using an adhesive under controlled conditions of a lamination device. Due to unique physical and mechanical properties of the constituents, their deformation behavior is more complex compared to bare metallic sheets, and especially with regard to the integrity of the polymer adherend-metal interface during forming processes. Consequently, there is much interest in understanding the interfacial adhesion strength (IAS) in such systems [Takiguchi and Yoshida, 2003; Takiguchi and Yoshida, 2004; Vayeda and Wang, 2007; van den Bosch et al., 2008; Huang and Wang, 2013].

Forming (plastic deformation) of PLSMs causes two simultaneous phenomena of (i) surface roughening of the metallic substrate and (ii) development of residual stress in the polymeric adherend. The metallic surface roughness is influenced by microstructural characteristics of the metallic material in forming conditions and residual stress is developed from a mismatch between physical and mechanical properties of polymeric and metallic constituents. Although both of these phenomena may lead to enhancement or deterioration in bonded strength, it is not clear as to what role each of them individually play in affecting IAS. In general, metallic substrate characteristics,

polymeric constituents of adherend (type of adhesive and polymer films and their mechanical properties), lamination parameters (pressure, temperature, etc.), amount and mode of deformation (such as stretching, bending, etc.) as well as forming speed are expected to govern the effects of deformation-induced residual stress and metallic surface roughness on the IAS. The overarching goal in design of a specific PLSM system (i.e., for a chosen metal substrate, polymer film and adhesive) is that no interfacial delamination and fracture of the component (or its constituents) should occur due to the forming process. More fundamentally, the energy stored in the adherend material due to the residual stress should be less than the interfacial adhesion energy due to the contact between the bonded materials; thereby the adherend materials do not delaminate upon deformation.

The metallic surface roughness can enhance the durability of adhesion with soft and conforming polymeric adherends mainly due to the increase in contact area [Chiche et al., 2000; Noori et al., 2015(a); van Tijum et al., 2007; Teixeira and da Silva, 2011]. It has been reported that adhesion durability can increase either from a decrease in delamination rate [Chiche et al., 2000] or from an increase in the force required for interface crack propagation [Noori et al., 2015(a)]. Alternatively, local interfacial delamination can be promoted at asperities on the surface that can result in IAS reduction [van Tijum et al., 2007]. It has been shown that rough surface with high amplitude asperities may weaken the interface during de-bonding due to large interfacial stress while uniform roughness with low amplitude results in more uniform stress distribution and hence stronger adhesion [Teixeira and da Silva, 2011]. The amplitude and spatial configuration of metallic surface roughness, thickness and mechanical properties of the polymer adherend materials and lamination process parameters are likely relevant factors that can govern the effect of surface roughness on IAS between polymer adherend and metallic substrate. The tensile residual stress, on the other hand, can result in interfacial

delamination upon relaxation of the residual stresses in bonded materials. A reduction in IAS by increasing the tensile residual stress has been observed by analyzing the peel and blister test results on mica-adhesive-aluminum bonded system [Jensen and Thouless,1993; Thouless and Jensen, 1994].

The effect of uniaxial deformation on adhesion between polymer film and sheet metal was investigated by using peel [van den Bosch et al., 2008] and pull-off tests [Huang and Wang, 2013]. Although a link between increased deformation and reduced IAS was established, the effect of substrate surface roughness was not isolated from the effect of deformation-induced residual stress on the adhesion loss. As the surface roughness effect could not be decoupled explicitly in their experiments, there is a clear need to devise new experiments to try to identify individually the roles of surface roughness and residual stress on IAS in deformed PLSMs to guide their design and development for forming applications.

This paper presents a new experimental methodology to isolate the effects of surface roughness and deformation-induced residual stress on interfacial peel strength (IPS) in uniaxially deformed PLSMs. Proposed methodology for determining the IPS is based on 180° peel testing of PLSM specimens prepared under two different lamination conditions, one involving systematic pre-straining in uniaxial tension of the metallic substrate prior to lamination and the other involving identical post-lamination pre-straining of the PLSM. Additionally, the effect of uniaxial pre-strain value and peel test speed, for the above laminations conditions, are critically analyzed for their effect on residual stress development, and consequently IPS, of two differently tailored PLSM systems.

2.2 Experimental procedure

Two types of polymer adherends were used to laminate on a stainless steel substrate with two different protocols as described below in section 2.2.2. The 180° peel test was conducted to evaluate the IPS between polymer adherend and metallic substrate. The details related to PLSM polymeric constituents, lamination and peel test procedures are given below.

2.2.1 Laminate constituent materials

Two types of polymer adherends, supplied by 3M Company (London, Ontario, Canada), involving a thin polymer film with a pre-applied acrylic pressure sensitive adhesive (PSA) were used in this study. Table 2.1 provides information about the two polymer adherends B and C that involved the same acrylic PSA but different films. The film for adherend B was bi-layer made from two different polymers. The film and adhesive thickness for both adherends were 0.091 mm and 0.036 mm respectively.

A bright-annealed ferritic stainless steel sheet (AISI 430) was used as the metallic substrate. The sheet metal substrate with 0.6 mm thickness was cut along its original rolling direction in the form of rectangular strips with a length of 100 mm and a width of 25.4 ± 0.1 mm. The cut edges were polished with a fine grit sand paper to eliminate the burrs. The width of the polymer adherend was kept the same as substrate while initial length was chosen to be 250 mm thereby providing a rise of 50 mm to peel arm length in 180° peel test. Polymer adherends were cut in compliance with the ASTM D 6287-05 standard to yield nick-free non-stretched specimens before lamination. Figure 2.1(a-c) illustrates the 180° peel test configuration and the samples geometry and Figure 2.1(d) shows de-bonded surfaces of metallic substrate and polymer adherend B after 180° peel test.

Table 2.1 3M™ adherend materials.

Adherend	Polymer film ^a	Acrylic PSA ^a
B	PE/PP copolymer with PET coating	Medium tack, high shear
C	PVC	

^a The polymer film and PSA layer thickness were 0.091 mm and 0.036 mm respectively.

2.2.2 Protocols for peel test sample preparation

Two different protocols, PAL and PBL, were devised for peel test sample preparation where the former acronym stands for pre-straining after lamination and the latter stands for pre-straining before lamination. PAL samples were prepared by first lamination of the adherend on as-received metallic substrate followed by uniaxial pre-straining of the PLSM to a range of pre-strain values. For PBL samples, the metallic substrate was pre-strained first to the same range of pre-strain values as PAL samples and then laminated with the adherend material.

Surface of the sheet metal was cleaned before lamination using acetone followed by a rinse with ethanol and drying with a lint-free cloth. Lamination was carried out using a roll laminator machine (Chemsultants International-Model HL-100, OH, USA) at 23°C. The roll laminator included two adjustable rollers (top roller as idler and bottom roller driven by a variable speed motor) to attain specific gap between them using two gauges at the two ends of the top roller. Two cylinders applied an adjustable air pressure to the top roller. Two layers of polymer adherends (instead of one layer) were applied to the sheet metal surface and lamination was carried out at a pressure and speed of 1700 kPa and 3-4 mm/sec respectively. Second adherend layer was used as an extra backing material during peeling to enhance the peel arm resistance to plastic or unstable deformation during peeling. A soft polyurethane pad of 2.5 mm thickness and 50 mm width with a durometer hardness of 40 OO was used between the top roller and the top

surface of the polymer film while maintaining 1.0 mm gap between the rollers. Polyurethane pad helped in improving the contact between PSA and substrate surface by providing a more uniform pressure distribution. After lamination, all PLSM samples were held in a vacuum container at ambient temperature of 23 °C for 30 days to stabilize the lamination condition.

Uniaxial tensile pre-straining was carried out using a computer controlled servo-hydraulic tensile machine at a speed of 2 mm/min. Seven pre-strain conditions of 0 (no pre-strain), 0.03, 0.04, 0.07, 0.09, 0.12 and 0.20 were applied to both PAL and PBL samples, all below the local necking strain of stainless steel substrate. Figure 2.2 shows the substrate surface roughness parameter (R_a) measured using an optical non-contact surface profilometer (Zygo-Model NewView 5000, CT, USA) for the range of pre-strain values. The measurements were conducted along the rolling direction of the metallic substrate over a field of view of 1.83×1.37 mm.

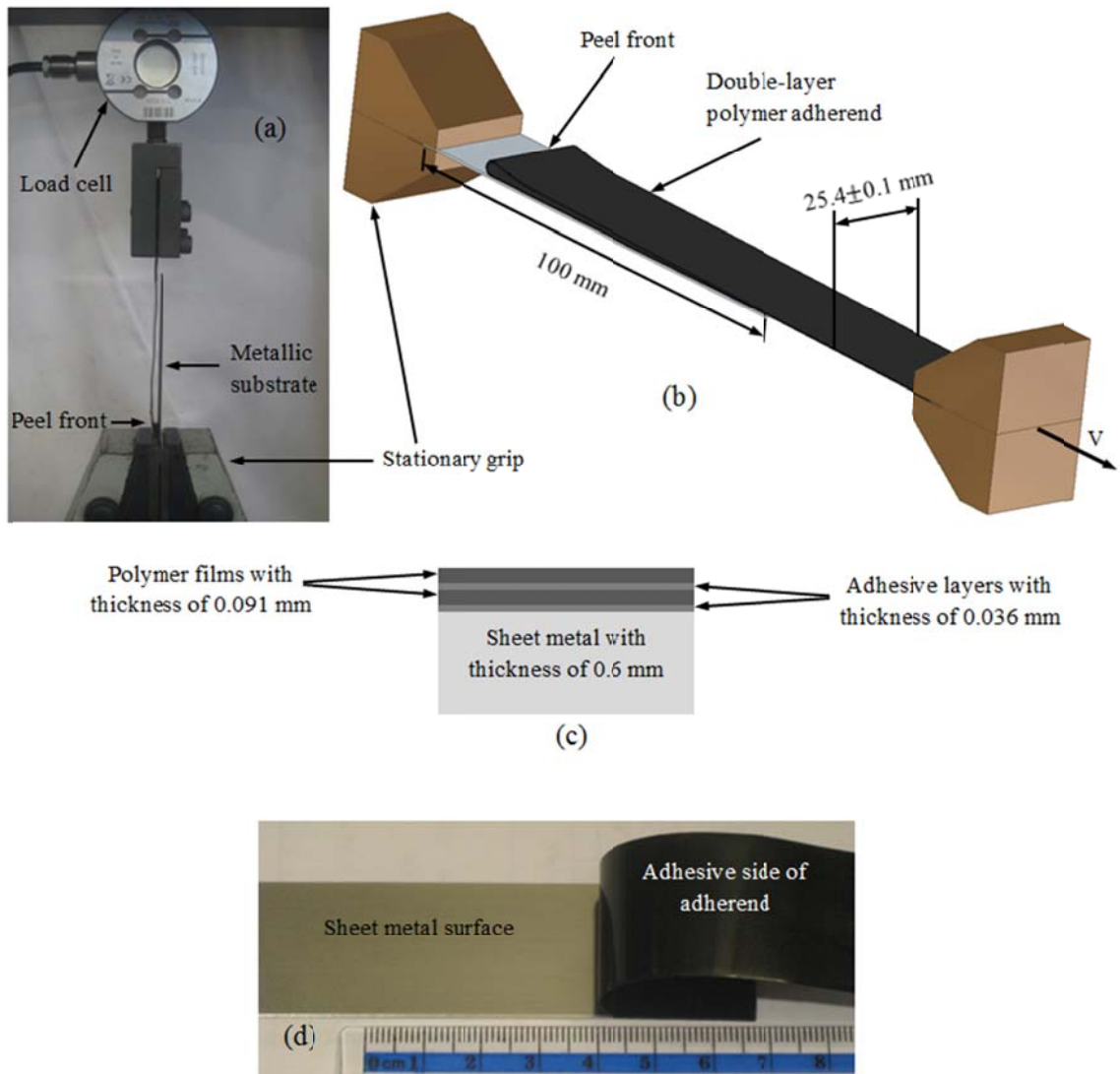


Figure 2.1 The 180° peel test configuration (a), a schematic of a peel sample, V shows the peel speed and direction (b), through-thickness geometry of the PLSM (c) and de-bonded surfaces of the sheet metal and polymer adherend B after 180° peel test (d).

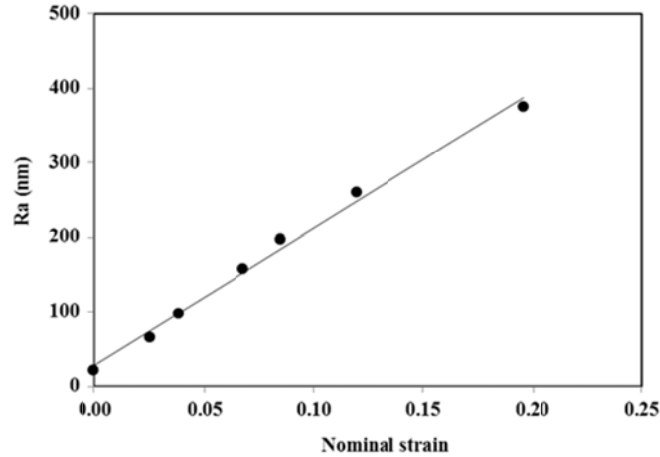


Figure 2.2 Surface roughness of metallic substrate (AISI 430) versus uniaxial tensile pre-strain value.

2.2.3 180° peel tests

The 180° peel tests were conducted by using a screw-driven tensile machine equipped with 2 kN load cell. The peel speed was chosen based on ASTM D 6862 standard for peel testing of adhesives in the speed range of 12-250 mm/min. The tests were performed at three cross-head speeds of 20, 100 and 500 mm/min, providing effective peel speeds of 10, 50 and 250 mm/min respectively which are the geometric sequences by the common ratio of 5. The steady-state peel force data from the test was normalized with test sample width, b , for comparison with variously pre-strained samples. The PAL samples were held for 7 days after uniaxial pre-straining, and prior to peel testing. Figure 2.3 shows a schematic of experimental steps for PAL and PBL samples. Table 2.2 summarizes the variables which their effects on IPS are presented in this paper.

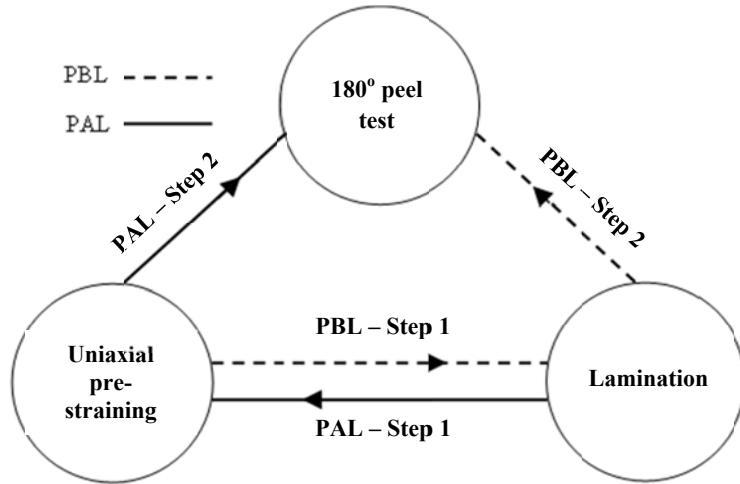


Figure 2.3 Flowchart representing the sequences for preparation and peel testing of PAL and PBL samples.

Table 2.2 The summary of peel tests variables.

Variable	Description
Sample preparation protocol (see Figure 2.3)	PAL (pre-straining after lamination) PBL (pre-straining before lamination)
Polymer adherend type (see Table 2.1)	Type B Type C
Uniaxial tensile nominal pre-strain value	0.03, 0.04, 0.07, 0.09, 0.12, 0.20
Peel speed	10, 50, 250 mm/min

2.2.4 Uniaxial tensile testing of adherends

The uniaxial tensile tests were carried out as per ASTM D 882 standard to obtain tensile properties of adherends under three different cross-head speeds, 10, 50 and 250 mm/min using Instron mechanical test system (model 3366, Canton, MA, USA). Adherend C was stronger and had a distinct yield stress peak in comparison to adherend B which was weaker and showed a smooth transition between elastic and inelastic parts (see Figure 2.4). Also, bi-layer adherend B exhibited an instantaneous drop in its stress-strain curves corresponding to failure of relatively brittle PET layer. Both films exhibited positive strain rate sensitivity as demonstrated by larger levels of stresses at higher cross-head speeds. Table 2.3 presents the initial yield strength (σ_y) and elastic modulus (E) of the polymer adherends at three different peel speeds which were obtained by the present authors in a separate study [Noori et al., 2015(b)].

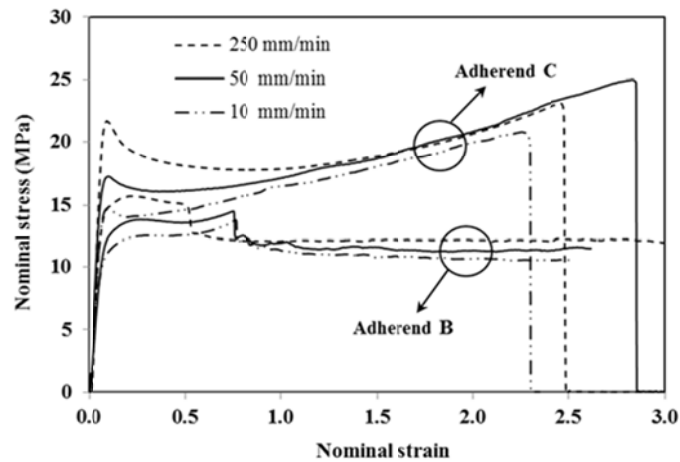


Figure 2.4 Nominal uniaxial tensile stress-strain curves for polymer adherends obtained at three different cross head speeds. The curves for 10 mm/min are from reference [Noori et al., 2015(b)].

Table 2.3 Mechanical properties of the peel arm at different uniaxial tensile test speeds [Noori et al., 2015(b)].

Peel speed (mm/min)	Adherend	σ_y (MPa)	E^* (MPa)
10	B	12.5	204
	C	14.6	309
50	B	13.8	239
	C	16.3	326
250	B	15.3	384
	C	18.9	617

2.3 Results and discussion

Results and discussion related to effects of polymer film, pre-strain magnitude and peel speed on IPS are presented in this section. Interfacial de-bonding occurred at the interface between the adhesive and metallic substrate in all test cases (see earlier Figure 2.1(d)). Figure 2.5 shows the normalized peel force (F/b) versus pre-strain value at three different peel speeds for the two PLSMs. Each data point represents the average of four test samples where the error bars indicate the range of data obtained at each condition. The accuracy of peel force measurement using a 2 kN load cell was compared with another smaller load cell of 50 N load capacity. These tests revealed a maximum difference of 2% in load measurement from the two load cells. In this paper, peel force results obtained from 2 kN load cell are reported for comparison between different testing conditions. The parameter (F/b) is half of the total energy (G) required for peeling based on a simplified, yet well-accepted, analysis of peel test (see eqn. (2.3.1) below) [Noori et al., 2015(b); Georgiou et al., 2003]. It is to be noted that peel angle θ takes a value of π for 180° peel test.

$$G = F(1 - \cos\theta)/b \quad (2.3.1)$$

The total peeling energy (G) is primarily composed of adhesion fracture energy and plastic deformation energy of the peel arm. The adhesion fracture energy is assumed to be a characteristic property of bonded interface and independent of properties of the polymer film [Noori et al., 2015(b); Georgiou et al., 2003] while the plastic deformation energy of the peel arm is influenced by both adhesion fracture energy and peel arm properties. Higher adhesion fracture energy promotes further plastic deformation of the peel arm thus contributing to the total required peeling energy.

2.3.1 Effect of adherend type on peel strength

Since lamination procedure, pre-strains, as well as type of acrylic PSA were the same for adherends B and C, quite similar interface characteristics and adhesion fracture energy between adhesive and metallic substrate were expected. However, adherend C required less peeling energy at all testing conditions compared to adherend B primarily because of its higher strength and thus lower plastic deformation during peeling (see Figure 2.4 and Table 2.3).

2.3.2 Effect of surface roughness on peel strength

Returning to Figure 2.5, one observes that PBL samples of both adherends B and C yielded almost constant peel force at each peel speed within the entire range of deformation-induced surface roughness of metallic substrate. Since the polymer adherends in PBL samples do not carry any deformation-induced residual stress before peel test, the results could be interpreted in terms of the effect of surface roughness alone on adhesion strength. Increasing the surface roughness can have dual effects on the adhesion strength, as discussed in the literature [Chiche et al., 2000; Noori et al., 2015(a); van Tijum et al., 2007; Teixeira and da Silva, 2011]. Increasing the contact area by increasing the surface roughness can promote mechanical interlocking between substrate

and adherend that is likely to increase the IAS. On the other hand, increasing the asperities amplitude can decrease the required energy for de-bonding through a change in the interfacial stress state during peeling. For the materials and testing conditions studied in this paper, it is inferred that neither of these two effects were dominant in peeling mechanism for PBL samples.

2.3.3 Effect of uniaxial deformation on peel strength

The combined effects of deformation-induced residual stress and surface roughness on peel strength of PLSMs were assessed using the results of PAL samples. After removal of uniaxial tensile forces in pre-straining stage, the sheet metal substrate is expected to recover its elastic strain immediately while the polymer adherend, with larger elastic strain component, is unlikely to recover all of its elastic strain due to the adhesion constraint of the metallic substrate. Therefore, tensile residual stress will remain in the polymer adherend in the loading direction. This residual stress is expected to reduce the IPS between the metallic substrate and adhesive as confirmed in Figure 2.5. The IPS of PAL samples was decreased by increasing the uniaxial pre-strain magnitude for both adherends at all peel speeds. In fact, after pre-straining and before peeling, the deformation-induced residual stress led to delamination of polymer adherend along the length at both free ends of PAL samples (see Figure 2.6). Delaminated areas increased with increasing the pre-strain magnitude for both adherends. Therefore, it can be inferred that increasing uniaxial pre-strain of PAL samples increases the residual stress in the polymer adherend.

For both adherends, the rate of decrease in IPS for PAL samples decreased with increasing the pre-strain value. This might be due to the fact that by increasing the pre-strain value, a larger fraction of the deformation energy will be dissipated through

permanent change in the polymer adherend microstructure. In other words, the residual stress did not increase linearly with pre-straining in PAL samples.

In addition to the effect of residual stress on delamination, a decrease in contact area might be another reason for weakening of the interfacial adhesion between the adhesive and metallic surface. In other words, deformation of PAL samples might result in some loss of interfacial contact between the adhesive and sheet metal substrate. If this is the case, then the IPS decreases not only due to the effect of residual stress but also due to the decrease in contact area. However, the effect of contact area on IPS can be overpassed by assuming that the contact area for PAL sample was the same as the corresponding PBL sample. This assumption, therefore, provides the maximum possible effect of residual stress on the IPS of PAL samples. As a result, the difference in normalized peel force of $(F/b)_{PBL} - (F/b)_{PAL}$, as presented in Figure 2.7, can be solely attributed to the effect of deformation-induced residual stress on adhesion of PAL samples. As shown in Figure 2.7, the $\Delta(F/b)$ value for adherend B is higher than that of adherend C suggesting that deformation-induced residual stress is more effective in decreasing the IPS of PLSMs of adherend B compared to adherend C. This might be due to the composite-type structure of the adherend B (see Table 2.1) which imposed through-thickness variation in mechanical properties. In contrast, adherend C, with a single layer of PVC film, was not subjected to through-thickness inhomogeneous deformation during pre-straining. The result is in agreement with the experimental observation of delamination at the edge of the PAL samples after pre-straining and before peeling. Adherend C showed less delamination at the edges of the peel samples compared with adherend B.

Figure 2.7 also includes a power law fit (using equation $\Delta(F/b) = He^m$) to the experimental data where parameter e represents the pre-strain value and the

constants H and m are fit parameters (see Table 2.4). The fit resulted in a correlation factor R of at least 0.985. The fitted curves can be utilized to assess the effect of residual stress on IPS at any pre-strain in the range of experimental pre-strains. Specifically, at $e = 0$ and for the PLSM samples with no pre-strain, $\Delta(F/b) = 0$ confirming that there is no deformation effect on the peel strength. Also, the rate of the function is decreasing with increasing pre-strain magnitude. This is in agreement with the data presented in Figure 2.5 for PAL samples where a decrease in rate of reduction of IPS with increase in pre-strain values is shown since a larger portion of the deformation energy will be dissipated by permanent change in the microstructure of the adherends.

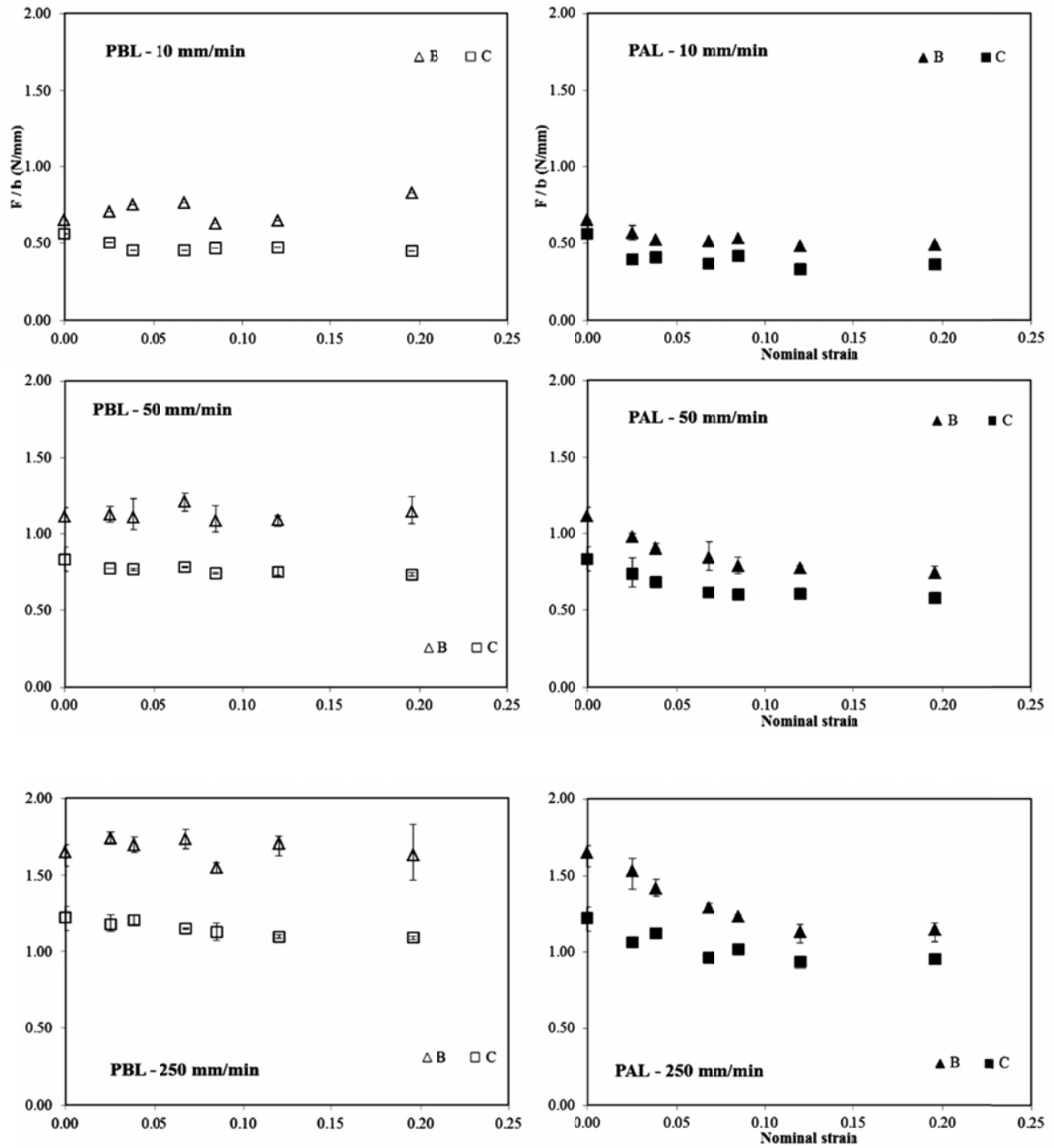


Figure 2.5 Normalized peel force versus pre-strain values for PBL and PAL samples at 10, 50 and 250 mm/min peel speeds.

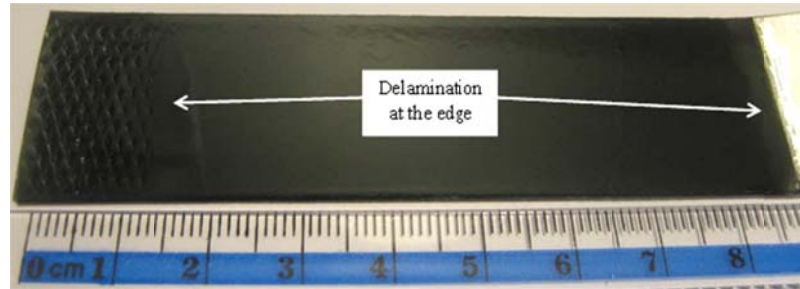


Figure 2.6 Delamination of the Adherend B from the edges of the PAL samples after pre-straining to the value of 0.07. The dents on the polymer surface at left hand side were caused by the tensile machine grips. The sheet metal substrate is hidden under the black polymer adherend.

2.3.4 Effect of peel speed on peel strength

The effect of peel speed on peel strength can be looked upon in terms of responses of the adherend constituents (PSA and polymer film). It is likely that the two constituents behave rather differently with respect to peel speed. Increasing the peel speed increases the IPS of the PSAs [Benedek, 2004] while it also strengthens the peel arm, as shown in Figure 2.4, which consequently increases the resistance of the peel arm to plastic deformation during peeling and therefore, decreases the IPS. For both adherends, increasing the peel speed raised the level of IPS, as shown in Figure 2.5, possibly exhibiting that the increase in peel resistance of the PSAs dominated the strengthening of the peel arm resistance to plastic deformation. In fact, it has been shown by current authors [Noori et al., 2015(b)] that increase in peel speed increased the plastic deformation of both adherend materials. Figure 2.8 shows the optical micrographs of the PET coating of adherend B, with no pre-strain, and after peeling at three peel speeds. During 180° peel test, the parallel lines were created on the film surface of adherend B. These lines were perpendicular to the peeling direction and included the micro-cracks

caused by deformation of the adherend. A higher peel speed increased the line density and thus the propensity for micro-cracking which is consistent with an increase in dissipated plastic deformation energy of adherend B. In contrast, Adherend C, involving a single layer PVC film, did not exhibit such microscopic features on the polymer surface during peeling. However, since both adherends had the same PSA, one can infer that the plastic dissipation energy of adherend C also increased with peel speed [Noori et al., 2015(b)].

The difference in IPS for PBL and PAL samples, $\Delta(F/b)$, of adherend B was increased with peel speed (see Figure 2.7 and Table 2.4). For adherend C, however, this difference increased with increasing the peel speed from 10 to 50 mm/min and decreased with increasing the peel speed from 50 to 250 mm/min. This shows that, for increasing the peel speed from 50 to 250 mm/min, the increase in IPS for PBL samples of adherend C was less than that for PAL samples. Although increasing the peel speed promotes the plastic deformation of the peel arm, larger deformation resistance of adherend C at higher peel speed decreased the rate of increase in IPS for PBL samples which consequently decreased the level of $\Delta(F/b)$ in Figure 2.7 at 250 mm/min peel speed.

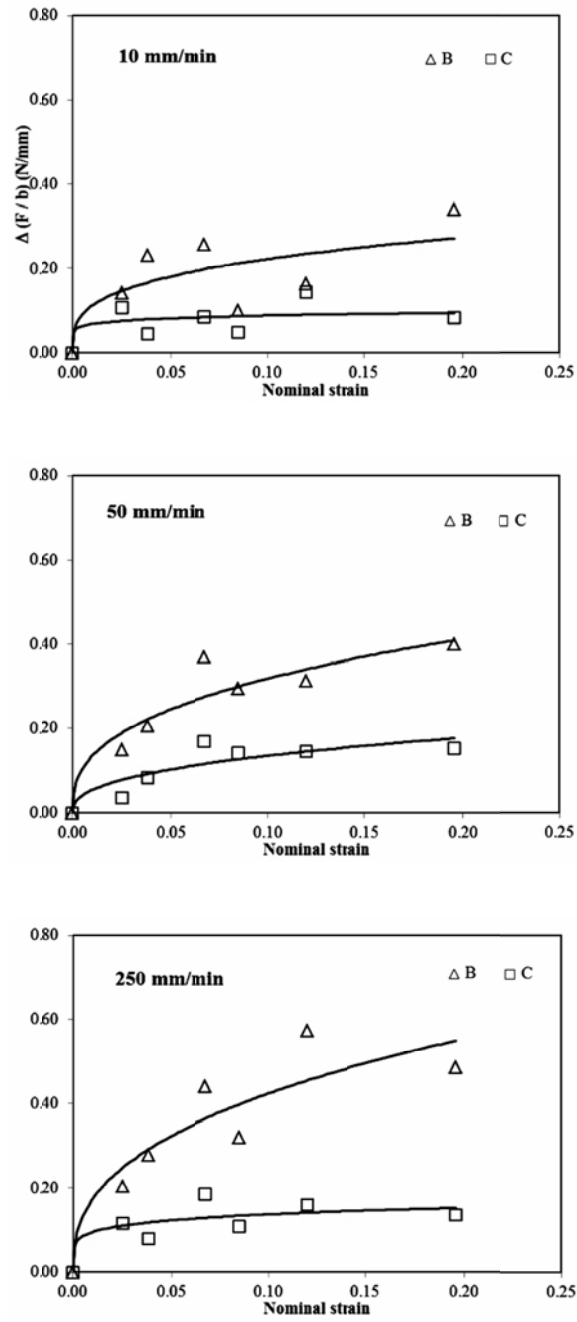


Figure 2.7 Difference of $(F/b)_{PBL} - (F/b)_{PAL}$ at different peel speeds.

Table 2.4 The constants H and m of power law equation for the fitted curves in **Figure 2.7**.

Adherend	Constants	Peel speed (mm/min)		
		10	50	250
B	H (N/mm)	0.442	0.758	1.032
	m	0.299	0.375	0.386
C	H (N/mm)	0.114	0.335	0.197
	m	0.110	0.393	0.156

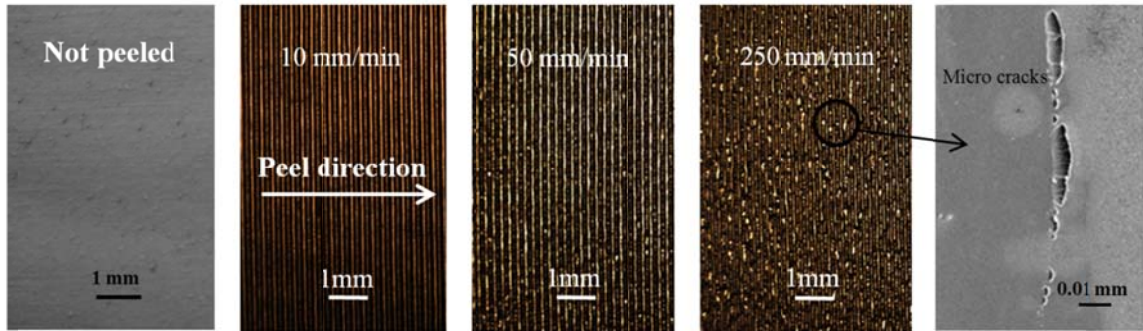


Figure 2.8 Microscopic views of the polymer surface showing the effect of peel speed on the peel arm of adherend B with no pre-strain. The far right image is a SEM micrograph and the rest are optical micrographs [Noori et al., 2015(b)].

2.4 Conclusions

Effects of deformation-induced residual stress and substrate surface roughness on peel strength of uniaxially deformed PLSMs were investigated by devising a new peel test

methodology that considered pre-straining of the substrate before lamination (PBL) and pre-straining of the PLSM after lamination (PAL). Experimental results related to effects of adherend type, deformation-induced surface roughness of metallic substrate, residual stress in polymer adherend and peel speed on interfacial peel strength (IPS) were presented and discussed.

The IPS of both adherends, with increase in tensile pre-strain magnitude decreased for PAL samples and remained almost constant for PBL samples. Uniaxial deformation showed less damaging effect on IPS of adherend C with a single layer of polymer film in comparison to adherend B involving a bi-layer polymer film. From a comparison of the PAL and PBL peel test results, it was established that adherend B experienced a larger deformation-induced residual stress after deformation compared to adherend C. This was in agreement with experimental observation of extent of edge delamination in PAL samples after deformation and before peeling.

The increase in peel speed increased the IPS for both adherends in PAL and PBL samples due to the enhancement of peel strength of PSAs with peel speed. The difference in IPS for PAL and PBL samples was monotonically increased with peel speed for adherend B while adherend C showed a maximum in this difference at medium peel speed of 50 mm/min.

2.5 Acknowledgements

The authors are thankful to Natural Sciences and Engineering Research Council of Canada (NSERC), Ontario Centre of Excellence (OCE) and 3M Canada for their financial support.

Chapter 3. Significance of Peel Test Speed on Interface Strength in Cohesive Zone Modeling

Abstract — The analysis of the experimental peel test data for obtaining the adhesion fracture energy of an adhesively laminated polymer to the sheet metal surface is considered. The experimental results of the 180° peel test on two types of polymer laminated sheet metal (PLSM) at three different peel speeds are analyzed by two methodological approaches in cohesive zone modeling. These approaches are linear-elastic stiffness approach and critical maximum stress approach. Comparing the results of these two approaches reveals the significance of the peel test speed on the interface strength determination for cohesive zone modeling. It is concluded that a “reference” peel speed may exist at which the interface strength is equal to the yield strength of the peel arm material. A constitutive equation has been proposed which relates the interface strength to the peel test velocity by using the reference peel speed and its corresponding peel arm yield strength.

Keywords: Peel; polymer laminated sheet metal; pressure-sensitive adhesive; analytical model; interface strength; peel speed

3.1 Introduction

The peel test is extensively used for determination of peeling energy between flexible laminates [Kinloch et al., 1994; Williams, 1997; Rahulkumar et al., 2000]. For plastically extendible peel arms, a proportion of the peeling energy is dissipated in the plastic deformation of the peel arm. Based on the energy balance, the adhesion fracture energy, G_c , can be potentially obtained by deducting the peel arm plastic deformation energy from the total peeling energy. The G_c is assumed to be a characteristic property of the interface and independent from the test method such as a standard LEFM test or an elastoplastic peel test [Hadavinia et al., 2006].

In recent years, cohesive zone models (CZMs) have been utilized for extracting the adhesion fracture energy from the total peeling energy. The CZM is based on a traction-separation (σ - u) relationship which is assumed to characterize the separation of the interface at the peel front. The traction-separation relationship is defined by two primary parameters which are the adhesion fracture energy (G_c) and the interface strength (σ_{max}). Figure 3.1, for example, shows a triangular form of the traction-separation relationship for the cohesive zone at the peel front. The σ_{max} is assumed to be a critical maximum stress in the damage zone ahead of the crack, k_s is the stiffness of the peeling material and b is the width of the peel arm. Although it has been shown that G_c , as obtained by CZM, is fairly insensitive to the form of the traction-separation relationship [Williams and Hadavinia, 2002], it is strongly dependent on the interface strength [Wei and Hutchinson, 1998]. Therefore, it is unlikely that an accurate estimation of adhesion fracture energy from peel test data can be made without prior information about interface strength.

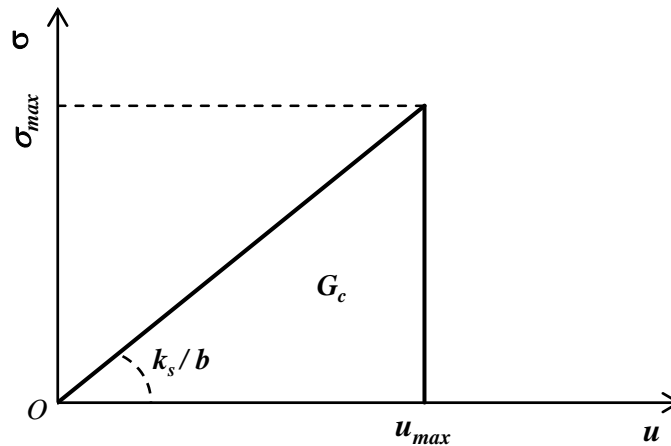


Figure 3.1 A triangular form of the traction-separation relationship for the cohesive zone at the peel front.

The estimation of the interface strength has been discussed for different interfaces by using the CZM [Wei and Hutchinson, 1998; Georgiou et al., 2003]. Based on the rate-independent separation laws, the estimation results show that the interface strength is dependent on the bond strength and is considerably larger than the yield strength of the peeling materials for strongly adhered materials. To address this issue, strain gradient theory for micro-scale yielding and geometrical constraints at the interface have been considered for providing some physical significance to the interface strength in CZM [Wei and Hutchinson, 1998; Georgiou et al., 2003]. However, such analysis has not resulted in reliable prediction of the interface strength prior to the analysis of peel data.

The effect of deformation rate on peeling energy has been discussed by Rahulkumar et al. [Rahulkumar et al., 2003]. Their work postulates a “characteristic peel velocity” which depends on geometry and intrinsic interfacial adhesion energy. At small and large peel speeds compared to the “characteristic peel velocity”, the peeling energy equals the intrinsic fracture energy. However, at the intermediate peel speeds, the viscous dissipation of the peel arm affects the peeling energy. In this case, they have suggested that a rate-dependent CZM needs to be utilized for analysis of peel test data.

This paper presents experimental evidence that the interface strength is not only dependent on peel arm material properties but also on peel test speed. For this purpose, the analytical solutions for rate-independent cohesive zone modeling of peel test by Georgiou et al. [2003] have been utilized to analyze the experimental data. The analytical solutions are based on two different approaches namely (a) linear elastic-stiffness approach and (b) critical maximum stress approach.

3.2 Experimental procedure

3.2.1 Materials and peel sample preparation

Two types of polymer laminated sheet metals (PLSMs) in the form of strips were prepared by laminating one side of the bright-annealed stainless steel sheets (AISI-430) with two types of polymer adherends supplied by 3M Company (London, Ontario, Canada). The polymer adherends were in the form of thin polymer film with a pre-applied acrylic pressure-sensitive adhesive (PSA) on one side. The compositional details of polymer adherends are presented in Table 3.1. The adherends involved the same adhesive type but two different polymer films. Adherend B involved a polypropylene (PP) and polyethylene (PE) copolymer layer which was sandwiched between a high gloss polyethylene terephthalate (PET) coat and the adhesive layer. Adherend C was a polyvinyl chloride (PVC) film with a pre-applied adhesive layer. Both adherends had the same polymer film thickness of 0.091 mm and adhesive layer thickness of 0.036 mm.

Adherend lamination to sheet metal substrate was carried out at 23°C by using a roll laminator (Chemsultants International-Model HL-100, Ohio, United States). The metallic substrate dimensions were 100 mm in length, 25.4 ± 0.1 mm in width and 0.6 mm in thickness. The width of the adherends was the same as the substrate width while the initial length was 250 mm giving rise to a peel arm length of 50 mm in the 180° peel test. For strengthening of the peel arm, an extra layer of the same polymer adherend with the same geometry was added on top of the laminated adherend. Therefore, the peel arm involving two polymer films and one adhesive layer between them had 0.218 mm thickness.

3.2.2 Peel test

The 180° peel test was conducted on PLSM samples by using a screw-driven tensile machine equipped with 2 kN load cell. Peel tests were performed at three cross-head speeds of 20, 100 and 500 mm/min, i.e., peel speeds of 10, 50 and 250 mm/min respectively. For comparison of results, the acquired steady-state peel force was normalized with the test sample width.

Table 3.1 3M polymer films and adhesives.

Adherend name	Polymer film ^a	PSA ^a (Acrylic type)
B	PE/PP copolymer + PET coat	High shear, medium tack
C	PVC	High shear, medium tack

^a The polymer film and PSA layer thickness were 0.091 mm and 0.036 mm respectively for both adherend materials.

3.2.3 Uniaxial tensile test

The uniaxial tensile tests were conducted for two adherend materials in accordance with ASTM D-882 standard and at 10, 50 and 250 mm/min cross-head speeds to be consistent with the peel speeds noted above. These tests were carried out by using an INSTRON tensile machine (Model 3366, Massachusetts, United States) with a ± 500 N load cell. Figure 3.2 shows a nominal stress-strain curve for the adherends at 10 mm/min cross-head speed. Adherend C involved stronger and more rigid PVC polymer compared to adherend B. The first drop in stress for adherend B is related to the rupture of high gloss PET coat of the adherend material. Increasing the tensile test speed increased the level of the stresses in stress-strain curves for both adherends.

For obtaining the yield strength required for peel data analysis, both films were assumed to be elastic perfectly-plastic and their yield strength was taken as an average of the yield stresses in the range of strains before the first drop in stress value for adherend B (i.e., e^* in Figure 3.2). This assumption was considered reasonable since the PET coat of adherend B did not show rupture during peeling experiment at all speeds.

Since two layers of polymer adherends were used in peel test sample preparation, the elastic modulus of the peel arm was calculated based on the iso-strain rule of mixture. The following relationship between total elastic modulus and number of layers in peel arm was obtained:

$$E = E_a \{ [N(\rho H + 1) - 1] / [N(H + 1) - 1] \} \quad (3.2.3.1)$$

where N is the number of layers, $\rho = E_f/E_a$, $H = h_f/h_a$ and the E_f and E_a are elastic moduli of polymer film and adhesive respectively. Similarly, h_f and h_a are thickness of polymer film and adhesive respectively. The derivation of equation (3.2.3.1) is presented in the Appendix.

The mechanical properties of the peel arm at different uniaxial tensile test speeds are presented in Table 3.2. The elastic modulus of typical PSAs is about 0.1-0.2 MPa at room temperature [Dale et al., 1989]. In this study, the elastic modulus of the adhesive layer is assumed to be 0.15 MPa at all peel speeds.

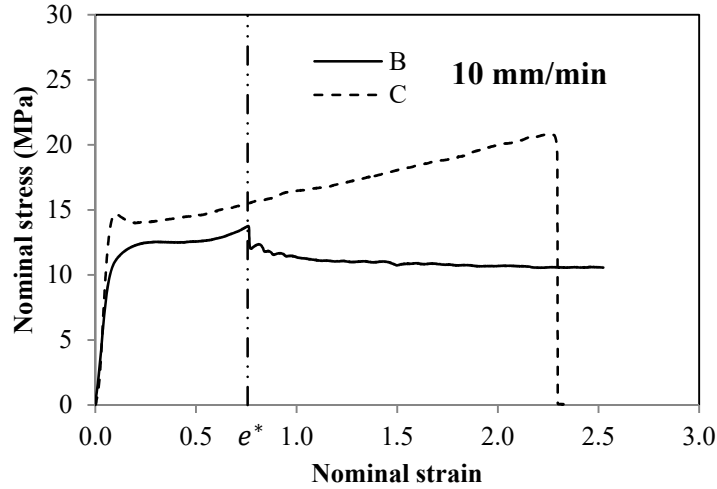


Figure 3.2 Nominal stress-strain curve for two adherend materials at 10 mm/min cross-head speed. The symbol e^* represents the nominal strain at which the nominal stress drops for adherend B due to the rupture of the PET coat on its top surface.

Table 3.2 Mechanical properties of the peel arm at different uniaxial tensile test speeds.

Peel speed (mm/min)	Adherend	σ_y (MPa)	E^* (MPa)
10	B	12.5	204
	C	14.6	309
50	B	13.8	239
	C	16.3	326
250	B	15.3	384
	C	18.9	617

* $N = 2$, $h_f = 0.091\text{mm}$, $h_a = 0.036\text{ mm}$ and E_a is assumed to be 0.15 MPa at all uniaxial test speeds.

3.3 Cohesive zone modeling of peel test

Figure 3.3 shows the schematic of the 180° peel test. Segment O-A represents the elastoplastic loading of the peel arm. Segment A-B is the elastic unloading and Segment

B-C represents the reverse plastic bending of the peel arm. In the elastoplastic loaded part of the peel arm, the parameter R is the radius of curvature at root rotation and δ is the characteristic length. The determination of δ is dealt with later in this section.

For obtaining the adhesion fracture energy from steady-state peel test data, the cohesive zone modeling method presented by Georgiou et al. [2003] has been implemented. The analysis is based on subtracting the energy dissipated due to the plastic deformation (G_d) of the peel arm from total peeling energy (G_t). Therefore, the adhesion fracture energy (G_c) would be simply obtained as:

$$G_c = G_t - G_d \quad (3.3.1)$$

Where $G_t = G + G_e$ and $G_e = \sigma_y^2 h / (2E)$ is the elastic energy release rate at fully plastic moment (M_p) for non-work hardening peel arm material. The parameters σ_y , E and h are the yield strength, elastic modulus and thickness of the peel arm respectively.

The total input energy for peeling is:

$$G = P(1 - \cos\theta)/b \quad (3.3.2)$$

where θ is the peel angle and b is the peel arm width. For the 180° peel test, $G = 2P/b$ since the displacement of the peel arm is twice of the peel front displacement. The plastic work done on peel arm before de-bonding from the substrate is [Georgiou et al., 2003]

$$G_d = P[1 - \cos(\theta - \theta_0)]/b \quad (3.3.3)$$

where $\theta_0 = \delta/R$ is the root rotation and is a crucial parameter in the analysis. The root rotation can be determined by the characteristic length of the deformation, δ , as shown in Figure 3.3 [Georgiou et al., 2003]

$$\theta_0 = 2\varepsilon_y k_0 (\delta/h) \quad (3.3.4)$$

where $\varepsilon_y = \sigma_y/E$ is the yield strain of the peel arm. The unknown parameter k_0 will be obtained during analysis by satisfying the global energy balance in peel test. The parameter k_0 corresponds to the stage at which the peel arm exhibits the minimum radius of curvature at the end of the bending process of the peel arm. The only remaining parameter in equation (3.3.4) for analysis is δ which can be obtained from two approaches referred to as (i) the linear-elastic stiffness approach and (ii) the critical maximum stress approach [Georgiou et al., 2003]. The former is based on LEFM where the cohesive zone is characterized by a single independent parameter which is adhesion fracture energy, G_c . For this approach, the critical maximum stress (σ_{max}) value is not required. In fact, it could be obtained from the analysis. On the other hand, the critical maximum stress approach requires two parameters to characterize the cohesive zone at the peel front, namely G_c and σ_{max} . This two parameters approach allows the CZM to deviate from LEFM in peel test analysis.

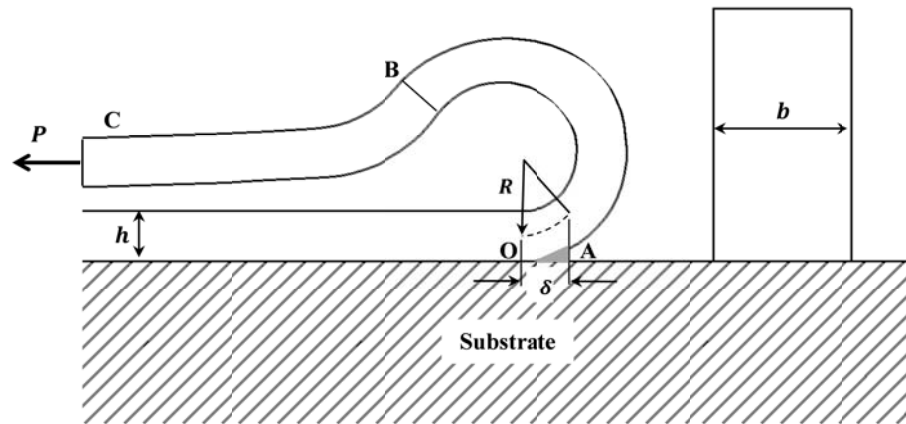


Figure 3.3 The schematic of the 180° peel test. The parameter R is the radius of curvature at root rotation and δ is the characteristic length.

Based on the linear-elastic stiffness approach, δ can be found from the following expression [Georgiou et al., 2003]:

$$(\delta/h)^4 = E[b/k_s]/(3h) \quad (3.3.5)$$

For half of the peel arm thickness and adhesive layer, $b/k_s = h/(2E_2) + h_a/E_a$ where E_2 is the transverse elastic modulus of the peel arm. Therefore, by neglecting the anisotropy through the thickness of the peel arm, $E = E_2$, equation (3.3.5) is simplified as:

$$(\delta/h)^4 = [1 + 2h_aE/(hE_a)]/6 \quad (3.3.6)$$

σ_{max} can be deduced at the end of analysis by combining equation (3.3.6) and definition of $G_c = \sigma_{max}^2(b/k_s)/2$ which is obtained from the area under the traction-separation curve (see Figure 3.1). Therefore, for isotropic peel arm material, σ_{max} can be obtained from the following expression:

$$\sigma_{max} = 2(EG_c/[h(1 + 2h_aE/hE_a)])^{1/2} \quad (3.3.7)$$

For the critical maximum stress approach, σ_{max} is assumed to be known for the analysis. Therefore, δ can be obtained from combining equation (3.3.5) and definition of G_c for the area under the traction-separation curve:

$$(\delta/h)^4 = 2EG_c/(3h\sigma_{max}^2) \quad (3.3.8)$$

In the present paper, a code called “ICPeel” (available in <http://www.me.imperial.ac.uk/AACgroup/index.html>, 2003) has been utilized which is written based on the above analysis. For both critical maximum stress and linear-elastic stiffness approaches, the inputs for the analysis is the thickness and elastic moduli of the adhesive and peel arm, yield strength and width of the peel arm, peel angle and steady-

state peeling force. Also, the interface strength, σ_{max} , is an extra input for the critical maximum stress approach. The outputs include G_t , G_c and G_d for both analytical approaches and also σ_{max} for the linear-elastic stiffness approach.

3.4 Results and discussion

3.4.1 Linear elastic stiffness approach

Table 3.3 presents G_t , G_c , G_d and σ_{max} obtained by linear-elastic stiffness approach for both polymer adherends at three different peel speeds. The values for G_t and G_c are higher for adherend B compared to those for adherend C at all three peel speeds. However, the value of G_d is almost the same for both adherends. Also, the interface strength obtained from linear-elastic stiffness approach for adherend B is slightly higher than that for adherend C.

Since both polymer adherends have the same adhesive layer, one may expect to obtain very similar results for adhesion fracture energy. However, Table 3 based on linear elastic stiffness approach, gives quite different value of G_c . This might be considered as a limitation of the linear-elastic stiffness approach whereby the plastic deformation energy is calculated first and then subtracted from the total peeling energy regardless of the type of the adhesive. Since, the peel arms for the two adherends have different tensile properties, the value of G_d is expected to be different. As a consequence, due to the weaker tensile properties of the peel arm made of adherend B (see Table 3.2), more plastic dissipation energy is expected for this adherend compared to the stronger peel arm made of adherend C. It has been observed by the experiments that the peeled arm of adherend B shows more elongation than that of adherend C under the same conditions of peeling. In contrast, the numerical results in Table 3.3 below show that at low and high peel speeds, the plastic dissipated energy is larger for adherend C. The

above results and analysis highlight limitations of using the linear-elastic stiffness approach.

3.4.2 Critical maximum stress approach

For analyzing the peel test data using the critical maximum stress approach, a value of pre-determined interface strength, σ_{max} , is required. For the determination of σ_{max} , the following methodology is devised based on three main assumptions. First, it is assumed that the adhesion fracture energies for both adherends are the same since they have the same adhesive layer between the polymer film and sheet metal substrate. Second, the adhesion between the adhesive and metallic surface is assumed to be weaker than that between the adhesive and polymer film. Third, it is assumed that both analytical approaches mentioned above should result in the same adhesion fracture energy, G_c . By utilizing these assumptions, the value of G_c obtained from the linear elastic stiffness approach for one of the adherends is considered as a reference value in the critical maximum stress analysis. Consequently, the value of σ_{max} will be obtained as an adjustment input parameter for the other adherend to satisfy the equality of the G_c values for both adherends within a tolerance range of ± 0.5 J/m².

Table 3.3 Analytical results for both adherends based on linear-elastic stiffness approach.

Peel speed (mm/min)	Adherend	G_t (J/m ²)	G_c (J/m ²)	G_d (J/m ²)	σ_{max} (MPa)
10	B	1313.5	861.9	451.6	2.7
	C	1128.5	667.1	461.4	2.4
50	B	2181.4	1602.2	579.2	3.7
	C	1678.4	1109.8	568.6	3.0
250	B	3409.2	2687.2	722.0	4.7
	C	2453.2	1722.5	730.7	3.8

3.4.2.1 Case I: Adherend B as a reference

Table 3.4 presents the results of critical maximum stress analysis for adherend C where the G_c for adherend B, which has been obtained from linear-elastic stiffness approach, is considered as a reference. For this purpose, the values of G_c for adherend B are taken from Table 3.3 for peel speeds of 10 and 50 mm/min. At these speeds, the values of both G_d and σ_{max} decrease with an increase in the peel speed. This is clearly in contradiction with the results obtained from linear-elastic stiffness approach. Also, smaller values of G_d at higher peel speeds, indicate that the peel arm behaves more elastically during peeling. In other words, this analytical case shows that if the speed is high enough, the adhesion tends to be weak and is unable to impose any permanent elongation in the peel arm during the separation from the substrate. This is in contradiction with the fact that the peel resistance of the PSAs increases with increasing peel speed [Benedek, 2004]. As shown in Table 3.4, at 250 mm/min peel speed, the numerical analysis did not converge to the corresponding value for G_c at any value of σ_{max} . Consequently, the G_d value could not be obtained for the maximum peel speed.

These unacceptable results might be due to the fact that the peel arm of adherend C is stronger than that for adherend B (see Table 3.2) and therefore, use of the linear elastic stiffness approach for adherend B to obtain the reference values for G_c cannot yield to the reasonable results for adherend C.

Table 3.4 Analytical results for adherend C based on critical maximum stress approach (case I).

Peel speed (mm/min)	G_t (J/m ²)	G_c (J/m ²)	G_d (J/m ²)	σ_{max} (MPa)
10	1128.5	861.8	266.7	1.0
50	1678.4	1602.5	75.8	0.3
250	2453.2	Not converged	Not converged	-

3.4.2.2 Case II: Adherend C as a reference

For this case, the values of G_c for adherend C based on linear-elastic stiffness approach are taken from Table 3.3 as the reference. The resulting adjusted values of interface strength for adherend B from critical maximum stress approach are presented in Table 3.5 where it is shown that the increasing of the peel speed increases the interface strength, σ_{max} .

In addition, the value of G_d , i.e., the amount of deformation of the peel arm is increasing with an increase in the peel speed. This is in agreement with the microscopic observations of the deformed surface of the peel arm for adherend B as shown in Figure 3.4. During peeling, a set of equally spaced parallel lines are evolving perpendicular to the peel direction. These features surface density increased with an increase in the amount of deformation at higher peel speeds. The parallel lines, as shown at top right of Figure 3.4, include elliptical micro cracks which their major axis is along the feature lines.

Table 3.5 Analytical results for adherend B based on critical maximum stress approach (case II).

Peel speed (mm/min)	G_t (J/m ²)	G_c (J/m ²)	G_d (J/m ²)	σ_{max} (MPa)
10	1313.5	667.0	646.5	5.6
50	2181.4	1109.9	1071.5	13.1
250	3409.2	1722.6	1686.6	31.4

As it is shown in Table 3.5, the interface strength of 13.1 MPa at 50 mm/min is rather close to the yield strength of 13.8 MPa of adherend B peel arm. This suggests that there might be a reference peel speed (V_{ref}) at which the interface strength is equal to the yield strength of the peel arm at that speed. Figure 3.5(a) shows the increase in yield strength and interface strength with increasing the peel speed. The least square curve fitting method is utilized to find the interception at which the yield strength and the interface strength will be equal and the corresponding speed is referred to as the reference peel speed.

Furthermore, there might be a relationship between the interface strength, peel arm yield strength and peel speed (V). Such a relationship can be mathematically expressed as:

$$\sigma_{max} = (\sigma_y)_{at V_{ref}} (V/V_{ref})^n \quad (3.4.2.2.1)$$

where the exponent of $n \approx 0.5$ was obtained by fitting the equation (3.4.2.2.1) to the normalized interface strength at different peel speeds, as shown in Figure 3.5(b).

The results of case II are in reasonably good agreement with the experimental observations and the PSAs peeling characteristics. The analysis of the peel test data by

using the critical maximum stress approach, as obtained from the “ICPeel” code, is independent of the value of the adhesive elastic modulus. Therefore, regardless of the rate-dependency of the PSA elastic modulus, the results presented in Table 3.5 and Figure 3.5 are promising and worthy of consideration.

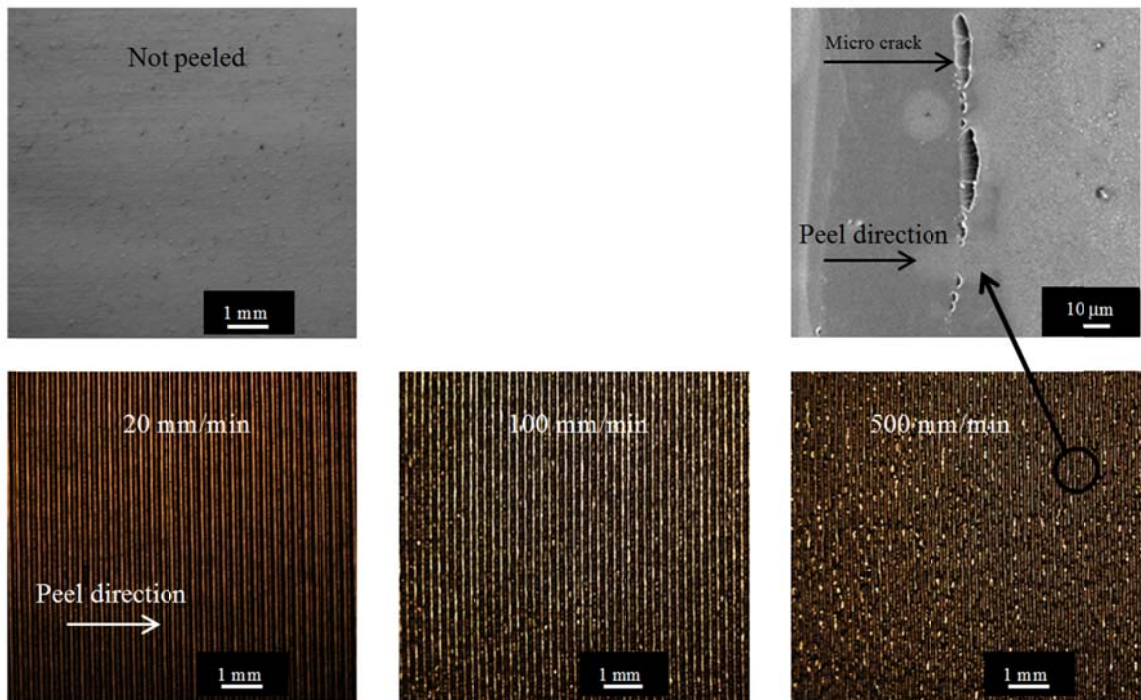


Figure 3.4 Microscopic views of the polymer surface showing the effect of peel speed on the peel arm of adherend B. The top right picture is the SEM micrograph and the rest are obtained by the optical microscope.

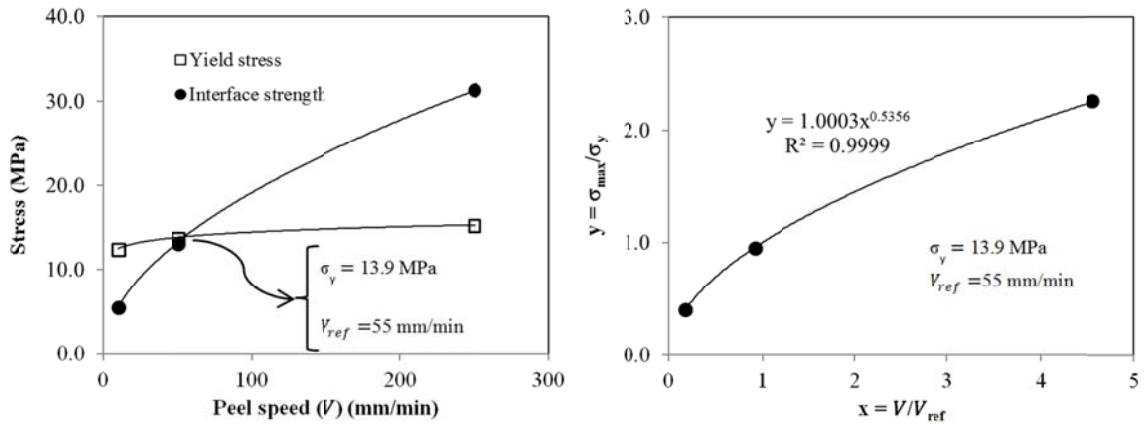


Figure 3.5 Yield strength and interface strength of adherend B with respect to the peel speed (a) and (b) fitted curve by using the least square method showing the relationship between interface strength, yield strength and peel speed based on equation (3.4.2.2.1).

3.5 Conclusions

The cohesive zone modeling results of peel test at different peel speeds are obtained from two rate-independent analytical approaches namely (a) linear-elastic stiffness approach and (b) critical maximum stress approach. Two types of peel test samples were prepared in which two different types of thin polymer films were bonded with the same type of PSA to the stainless steel substrate. The modeling results as presented in Table 3.5, assuming identical adhesion fracture energy for both adherends, might be considered useful for the determination of interface strength in cohesive zone modeling of peel test.

The results suggest that a “reference” peel speed might exist at which the interface strength is equal to the yield strength of the peel arm. For the bonded materials in this study, a rather simple yet practical constitutive equation has been proposed which relates the interface strength to the peel speed and yield strength of the peel arm at the reference peel speed. This proposed constitutive equation can be utilized toward the

development of a rate-dependent cohesive zone model for determination of the adhesion fracture energy between bonded materials. Exploring the wider applicability of this equation for the other types of bonding materials and interfaces can be considered by researchers for their studies.

3.6 Appendix A

In peel arm, for N number of layers of adherend, there are $N - 1$ layers of adhesives. The total force (F_t) applied on the adherend is obtained as follows:

$$F_t = NF_f + (N - 1)F_a \quad (3.6.1)$$

where F_f and F_a are the forces carried by the film and adhesive layers respectively and could be replaced with the corresponding stresses and areas (since $F = \sigma A$). By assuming the same width for polymer film and adhesive layer and based on the iso-strain rule of mixture, Equation (3.6.1) can be simplified to obtain the elastic modulus of the peel arm (E):

$$Eh = NE_f h_f + (N - 1)E_a h_a \quad (3.6.2)$$

where $h = Nh_f + (N - 1)h_a$. Equation (3.2.3.1) is obtained from equation (3.6.2) by defining $\rho = E_f/E_a$, $H = h_f/h_a$.

Chapter 4. Influence of metallic substrate surface engineering on peel resistance of adhesively bonded polymer film

Abstract — The peel resistance of adhesively bonded polymer films to a stainless steel sheet substrate (SSSS) with different engineered surface characteristics was examined in two different loading directions and for two different peel speeds. The SSSS was laminated with two thin polymeric adherends using two different pressure-sensitive adhesives. The SSSS surface was altered by grinding and knurling techniques before lamination and the effects of surface alterations on peel resistance was compared with peel resistance of the adherend from as-received SSSS with a bright-annealed surface condition. For ground surface, an increase in adherend peel resistance was observed and the increase was attributed to increase in contact area between the adhesive and SSSS surface. For knurled surfaces which involved deeper and less frequent grooves, however, a decrease in peel resistance was observed. This was attributed to a more complex stress state at the peel front in the SSSS groove region during peeling. An increase in peel speed enhanced the peel resistance from both ground and knurled surfaces.

Keywords: adhesively bonded polymer film; pressure-sensitive adhesive; metallic substrate; surface engineering; peel test.

4.1 Introduction

The adhesion of polymers to metals is of increasing interest in applications where there is a need for the unique properties of both metals and polymers. The basic research interest in polymer-metal adhesion has been driven by the new trend in manufacturing of lighter, more durable and environmentally friendly products and devices. In this regard, much effort has also been devoted to enhancing the adhesion through improving the bonding procedures and techniques. Surface engineering of the adhered materials before bonding is a common method for strengthening the adhesion between polymers and metals.

Chemical treatment and mechanical alteration of the surface are the two primary research avenues that have been pursued in the literature.

The chemical treatment of the adherend materials surface is often utilized to change the chemical composition of the surface(s) resulting in better coherency between the adherend at the interface. For instance, Lee and Qu [2003] oxidized the copper-based alloy with hot alkaline solution to roughen the substrate surface by creation of pebble-like and needle-like precipitates of Cu_2O and CuO respectively. The increase in oxidation time up to 10 minutes increased the surface roughness of the substrate from 0.030 to 0.120 μm . Sandwich double cantilever beam test results showed that, in general, the surface roughness of the black oxide coating enhanced the adhesion with epoxy molding compound by increasing the interfacial mechanical interlocking and increasing the cohesive failure proportion in the polymer. In another work, Chan et al. [2007] studied the adhesion between soft, elastomeric interfaces of polydimethylsiloxane (or PDMS) where the surfaces were modified by two-dimensional surface patterning that involved a periodic variation in chemical composition. By using 90° peel test, they showed that peel resistance could be optimized by controlling the spatial distribution of surface patterns.

Mechanical alteration of the adherend surface(s) with no change in surface chemical composition offers another possibility of enhancing the adhesion between polymer film and metal substrate. For example, Fabrin et al. [2007] used the injection molding technique for adhering the thermoplastic elastomer to the engineered surface of a pure aluminum sheet. The original rolled surface of the aluminum sheet was etched with different etching regimes and the elastomer peel resistance was evaluated by 180° peel test. They reported the increase in peel resistance due to the increase in contact area caused by surface chemical etching.

In another investigation [Rincon Troconis and Frankel, 2013], the effect of surface abrasion of AA2024-T3 aluminum alloy on its adhesion to polyvinyl butyral

coating was evaluated by the blister test. The aluminum surface was abraded by using different SiC grit papers in two configurations of grooves with randomly and aligned orientations. The average surface roughness was in the range of 0.026-1.326 μm . The increase in adhesion resistance with increasing surface roughness was attributed to increase in contact area. This increase in adhesion resistance was more for randomly oriented grooves configuration compared to the aligned grooves pattern.

Watts and Castle [1984] used the so-called cathodic disbondment test from British Gas Specification PS/CW6 to assess the adhesion of epoxy to the mild steel substrate. The surface of mild steel was treated by four techniques of polishing, abrasion, chemical agitation, and grit blasting resulting in surface roughness values of 0.05, 0.85, 1.70, and 3.80 μm , respectively. In this study, the predominant failure mode for all surface conditions was interfacial adhesive fracture. However, cohesive failure proportion increased with an increase in substrate surface roughness.

Azari et al. [2010] investigated the influence of metallic substrate surface roughness on fatigue and fracture behavior of a toughened epoxy adhesive by testing double cantilever beam specimens made from adhesively bonded AA6061-T651 aluminum bars. The metallic surface was abraded by sandpaper and grinding disc to obtain surface roughness values in the range of 1.3-9.0 μm . It was reported that fatigue resistance for dominant interfacial fracture mode was promoted by increasing the surface roughness and then reached a plateau followed by a decrease for the very rough surfaces. The increase in fatigue resistance was attributed to the increase in contact area, crack growth retardation due to micro-topography and crack path deviation from the interface. The decrease in fatigue resistance, on the other hand, was attributed to void formation and stress concentration at the tip of asperities. When the crack path was far enough from the interface or the proportion of cohesive fracture increased, the substrate surface roughness did not significantly influence the fatigue and fracture resistance of the joints.

In another study, the adhesion of roughened AA2024-T3 with a heat resistant adhesive was investigated using single-lap shear test [Cho et al., 2009]. The surface of the aluminum substrate was roughened by sand blasting to produce the surface roughness values in the range of 1.83- 6.82 μm . The surface was also milled to obtain a surface roughness of 0.32 μm . It was reported that as the surface roughness increased, the effective contact area increased resulting in an increase in shear strength except for a very rough surface which led to a slight decrease in shear strength. The decrease in shear strength was attributed to the decrease in cohesive failure area.

The present study deals with peel resistance of two thermoplastic polymer adherends from mechanically altered surface of AISI-430 ferritic stainless steel sheet substrate (SSSS). The polymer adherends were laminated on SSSS using two different acrylic pressure-sensitive adhesives (PSAs). The SSSS surface conditions were altered by grinding and knurling of the as-received bright-annealed surface of SSSS.

4.2 Experimental procedure

The 180° peel test samples were prepared in the form of polymer laminated sheet metals (PLSMs). The details of sample preparation were as follows:

4.2.1 Materials and peel test sample preparation

Two types of PLSMs in the form of strips were prepared by laminating one side of SSSS with two types of polymer adherends supplied by 3M Canada (London, Ontario, Canada). The polymer adherends, namely HGF and LGF, were in the form of thin polymer film with a pre-applied acrylic PSA on one side. Figure 4.1 shows a schematic of the PLSM strip and Table 4.1 provides compositional details of polymer adherends.

The adherend HGF involved a polypropylene (PP) and polyethylene (PE) copolymer layer which was sandwiched between a high gloss polyethylene terephthalate

(PET) coat and the adhesive layer with high tack and medium shear properties. The adherend LGF was a polyvinyl chloride (PVC) film with a pre-applied adhesive layer with medium tack and high shear properties. Both adherends had the same total thickness of 0.127 mm and adhesive layer thickness of 0.036 mm.

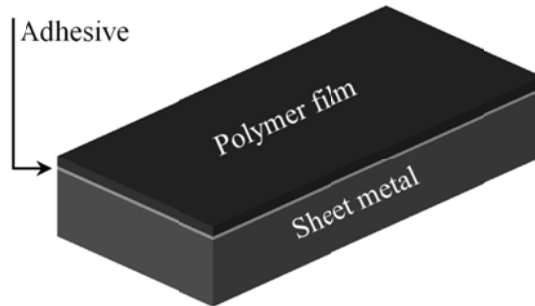


Figure 4.1 A schematic of the PLSM strip.

Table 4.1 3M polymer films and adhesives.

Adherend name	PSA ^a (Acrylic type)	Polymer film ^a
HGF	High tack, medium shear	PE/PP copolymer + PET coat
LGF	High shear, medium tack	PVC

^a The PSA layer and polymer film thickness were 0.036 mm and 0.091 mm respectively for both adherend materials.

Adherend lamination to SSSS was carried out at 23°C by using a roll laminator (Chemsultants International-Model HL 100). The metallic substrate dimensions were 100 mm in length, 25.4 ±0.1 mm in width. The width of adherends was the same as substrate width while the initial length was 250 mm giving rise to peel arm length of 50 mm in the 180° peel test. The nick-free and non-stretched polymer adherends were prepared by cutting the adherends in compliance with the ASTM D 6287 standard. In

order to facilitate the conformation of the adherend to the surface features of metallic substrate, a soft polyurethane pad (with durometer hardness of 40 OO) with 2.5 mm thickness and 50 mm width was used between the top roller and the polymer film to distribute the laminating pressure of approximately 1700 kPa uniformly over the top surface of polymer film. After lamination, the samples were held in vacuum bags at ambient temperature of 23 °C for four weeks to stabilize the interfacial bonding before peel testing.

As-received SSSS had a thickness of 0.6 mm and bright annealed surface condition with an average surface roughness (R_a) of 0.03 μm in rolling direction and 0.04 μm in transverse direction (i.e. perpendicular to rolling direction in the sheet plane). Two mechanical surface modification techniques, namely grinding and knurling, were utilized to change the surface characteristics of SSSS before lamination, as described below.

4.2.1.1 Grinding

The surface roughness of SSSS of size 610 mm \times 305 mm was changed by utilizing a CNC grinding machine. A 330.2 mm diameter ceramic grinding wheel made from Al_2O_3 with a speed of 400 rpm was used. The SSSS was firmly fixed on a magnetic platform and the surface of the sheet metal was scanned four times by the grinding wheel with a 101.6 mm/min feed rate. Thereafter, the samples with 25.4 ± 0.1 mm width and 100 mm length were cut parallel and perpendicular to the grinding direction. The samples were cut by metal shearing machine in which adequate sheet holding force was applied by plastic holding shoes during cutting to prevent any damage to the sheet metal surface. The sample edges were subsequently deburred and polished with ANSI 600-grit (13.0-16.0 μm) sandpaper. The surface roughness pattern of the ground sheet metal was measured by a non-contact optical surface profiler (Zygo-Model NewView 5000) in parallel and perpendicular directions with respect to the grinding direction. Figure 4.2 shows the stereoscopic image and a three-dimensional (3-D) representation of the ground

surface features with average roughness (R_a) value of $0.65 \mu\text{m}$ perpendicular to the grinding direction. After polishing the cut edges, the samples surfaces were cleaned with acetone and subsequently rinsed with ethanol prior to lamination with polymer adherend material.

4.2.1.2 Rolling the sheet metals with a redesigned knurling tool

Knurling tool is conventionally used for making patterns on round pieces manually or by the lathe. For the present study, knurling tool was used for printing a pattern on SSSS surface. For this purpose, a one-roller knurling tool was designed and installed on a milling machine. By locking the head of the machine and moving the table, the knurling tool was able to print a groove pattern of interest on the surface of SSSS. For this purpose, SSSS of size $610 \text{ mm} \times 178 \text{ mm}$ was held on a table using several vises, while its surface was scanned by the knurling roller with a width of 6 mm . Figure 4.3 shows the stereoscopic image of the knurled surface and a 3-D representation of one knurled groove with an average depth of $15 \mu\text{m}$ measured with Zygo optical surface profiler. After printing the pattern, samples were cut in parallel and perpendicular directions with respect to knurling direction and laminated by following the same procedure utilized for ground SSSS. Besides the above two sets of peel samples involving ground and knurled substrate, one more set of peel samples was prepared by laminating as-received bright-annealed SSSS samples with polymer adherends. For this surface condition, the test specimen length was along the original rolling direction of SSSS and influence of test specimen orientation was not explored.

4.2.2 Peel test

The 180° peel tests were conducted on four replicate PLSM samples at each peel condition by using a screw-driven tensile machine equipped with 2 kN load cell. Peel tests were performed at two cross-head speeds of 100 and 500 mm/min , providing

effective peel speeds of 50 and 250 mm/min, respectively. The steady-state peel force data from each test were normalized with test sample width (b). Figure 4.4 shows the steady-state peel zone on a typical peel test curve. The average of four normalized peel forces is reported for each test condition.

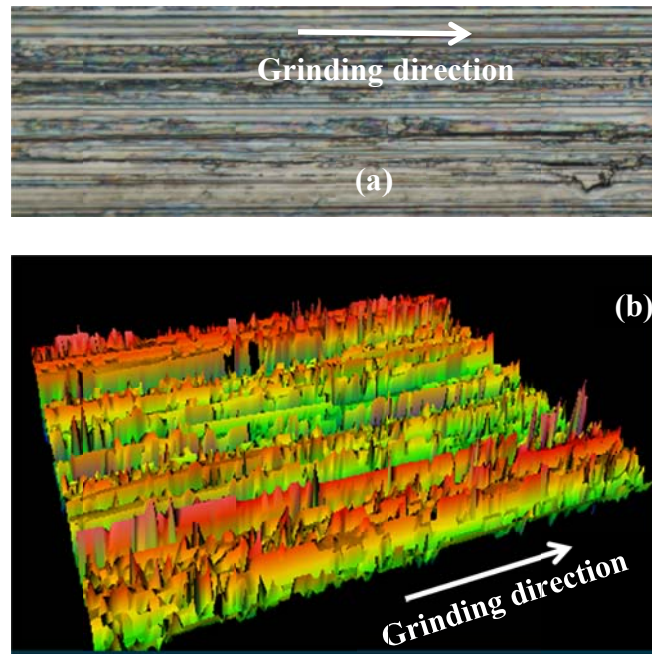


Figure 4.2 Images of the ground surface, (a) stereoscopic image from optical microscope, (b) 3D image from Zygo optical surface profiler.

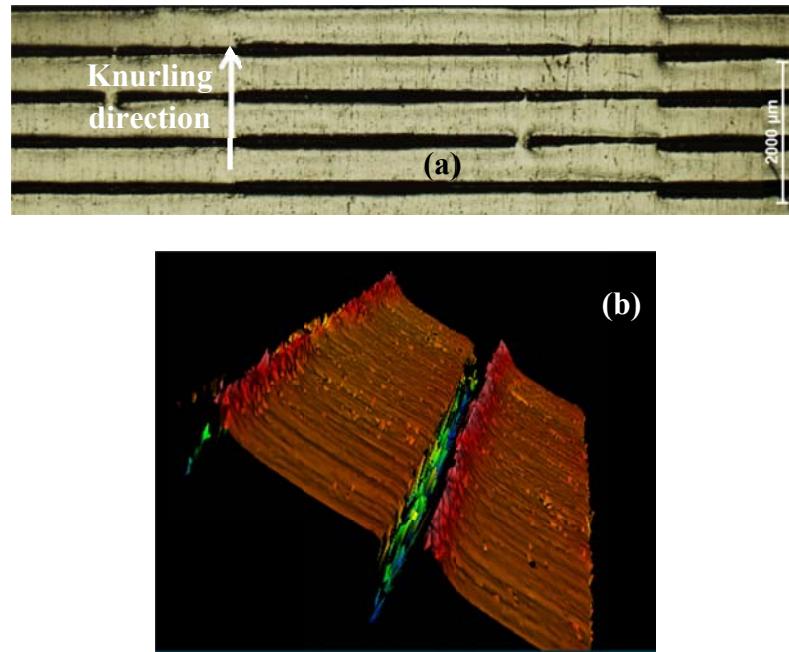


Figure 4.3 Images of the knurled surface, (a) stereoscopic image from optical microscope (bright annealed surface is visible in areas adjacent to the dark groove region), (b) 3D image from Zygo optical surface profiler.

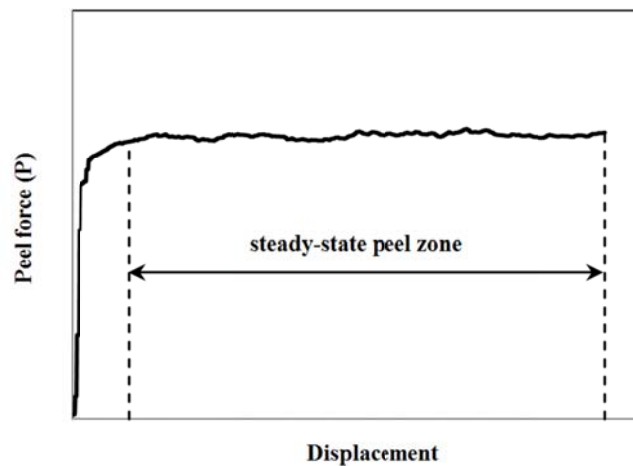


Figure 4.4 A typical peel force versus displacement trace from experiment showing steady-state peel zone.

4.3 Results and discussion

For assessment of the effect of substrate surface modification on peel results, the significance of difference in normalized peel force at various conditions was examined by using the statistical analysis at 95% confidence level. Figure 4.5 shows a comparison of normalized peel force from ground and bright annealed surface of SSSS where the error bars indicate the range of normalized peel force data obtained for each condition. For ground surface, the peel tests were conducted along and perpendicular to the grinding direction. As shown, for all surface conditions and peel speeds, the normalized peel force was less for adherend LGF compared to HGF due to lower tack properties of PSA for adherend LGF. For both adherends, the normalized peel force was larger for 250 mm/min peel speed compared to 50 mm/min for all surface conditions. This result was consistent with literature in terms of increase in peel resistance of the PSAs with increase in peel speed [Benedek, 2004].

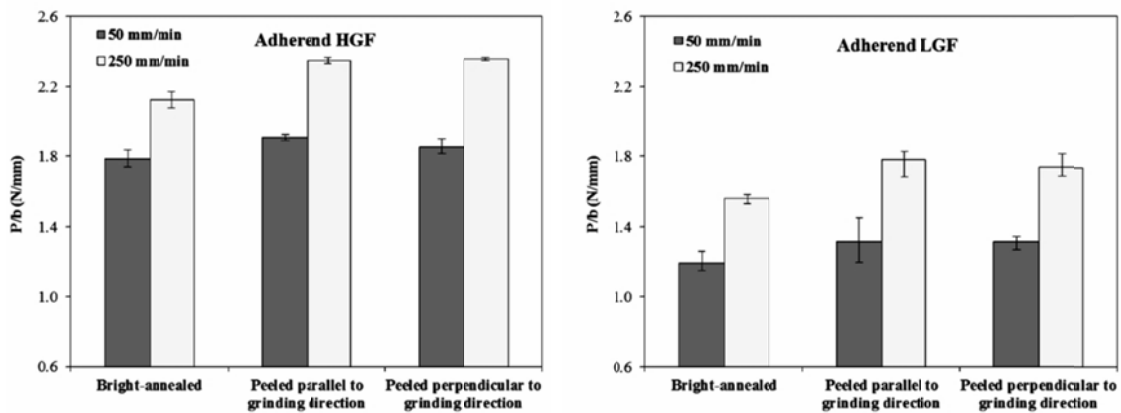


Figure 4.5 Normalized steady-state peel force of adherends HGF and LGF from ground and bright-annealed surfaces at two peel speeds.

The average normalized peel forces from ground SSSS in parallel and perpendicular directions to grinding direction were similar and consistently higher than for the bright annealed condition. Thus, surface alteration by grinding effectively enhanced the average peel resistance of the adherends regardless of properties of PSAs and also direction of peeling. Figure 4.6 shows the scanning electron micrograph of the through-thickness interface between pre-applied adhesive of HGF adherend and SSSS with a roughness of $0.65 \mu\text{m}$. The asperities on the metallic substrate surface were covered by the adhesive layer and thus the interfacial contact area was increased. The increase in contact area, and therefore, increased mechanical interlocking between the adhesive and ground SSSS surface is likely the cause of increased peel resistance. The similarity between normalized peel forces along and perpendicular to grinding direction is attributed to the uniform spatial distribution of the microscale asperities on the ground SSSS surface (see Figure 4.2).

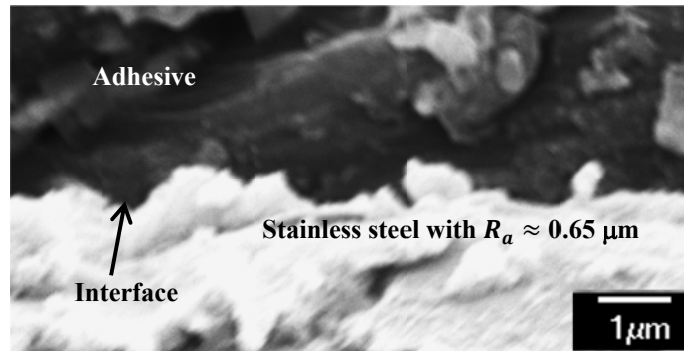


Figure 4.6 Scanning electron micrograph shows the through-thickness interface of the adhesive and SSSS, the latter with an average roughness value of $0.65 \mu\text{m}$.

It is noteworthy that the increase in peel resistance for ground SSSS surface was higher at larger peel speed of 250 mm/min . For adherend HGF, the increase in average normalized peel force for ground SSSS compared with bright annealed surface condition

was about 0.10 N/mm (6%) at 50 mm/min speed and about 0.22 N/mm (10%) at 250 mm/min whereas, for adherend LGF, the average increase was 0.12 N/mm (14%) at 50 mm/min and 0.20 N/mm (16%) at 250 mm/min. This increased peel force at higher speed was contributed by the increase in peel resistance of PSA and also increase in plastic deformation of the adherend during peeling. Figure 4.7 shows the stereoscopic images of the top surface of the HGF adherend after peeling at two different peel speeds. The vertical line features on the surface of polymer films were caused by plastic deformation of the adherend during peeling and included the micro-cracks along the features. Higher areal density of vertical lines is indicative of the increased plastic deformation of the adherend at higher peel speed.

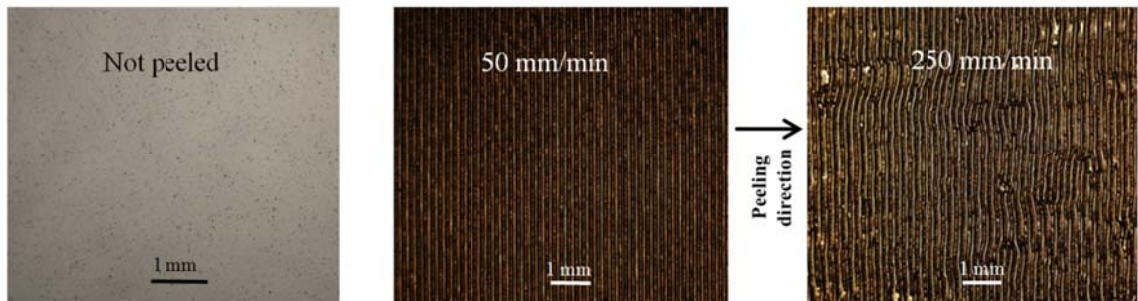


Figure 4.7 Stereoscopic images of top surface of adherend HGF before and after peeling at 50 and 250 mm/min peel speeds.

Figure 4.8 shows a comparison between normalized peel forces for knurled and bright annealed surface conditions. The grooves on knurled surfaces were much deeper than on ground surfaces. As mentioned earlier, the knurled grooves had the average depth of 15 μm which was comparable with the adhesive thickness of 36 μm . In this case, deep grooves deteriorate the peel resistance through either decrease in actual bonding area between the PSA and substrate or by changing the stress state at the near-

vertical wall surface of the knurled grooves (see Figure 4.3(b)) to reduce the peel force. This explanation is supported by literature in that the surface roughness changes the interfacial stress state which may cause reduction in de-bonding resistance for very rough surfaces.[Persson and Tosatti, 2001; Sancaktar and Ma, 2009]. It is likely that new stress components are developed during peeling at inclined walls of each groove and therefore resulting in a decrease in the required peel force at the interface.

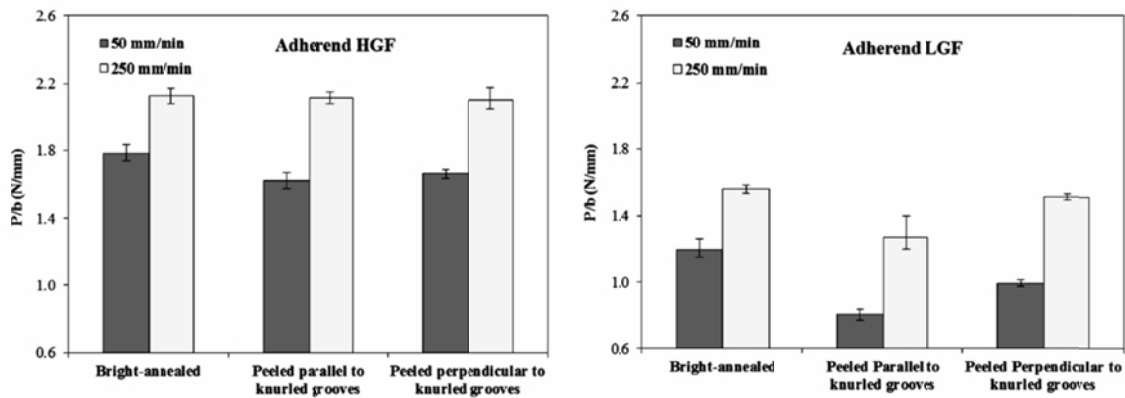


Figure 4.8 Normalized steady-state peel force of adherends HGF and LGF from knurled and bright-annealed surfaces at two peel speeds.

Table 4.2 provides the difference in peel resistance of the adherends from knurled and bright annealed surfaces at different peel conditions. In accordance with the above discussion, the normalized peel force at 50 mm/min peel speed was less for knurled surface compared to the bright annealed surface for both adherends. However, the difference in peel resistance for adherend HGF was not significant at high peel speed of 250 mm/min. It is inferred that the increase in peel speed could compensate the deterioration effect of the knurled surface on peel resistance of the high tack adhesive involved in HGF adherend.

For adherend LGF, however, the normalized peel force for tests along the length of the grooves (parallel to the knurled grooves) was less compared to the force along the width of the grooves (perpendicular to the grooves length) at both peel speeds (30% at 50 mm/min and 20% at 250 mm/min). On the other hand, the normalized peel force for adherend HGF involving PSA with higher tack properties, was not sensitive to the test direction from knurled SSSS surface (see Figure 4.8). Increasing the peel speed did not change the influence of test direction on the normalized peel force for both adherends for the knurled SSSS surface.

Table 4.2 Decrease in peel resistance of adherends from knurled surface compared with bright-annealed surface at two peel speeds.

Peel condition	Peel speed (mm/min)	Adherend HGF				Adherend LGF			
		parallel to the knurled grooves		perpendicular to the knurled grooves		parallel to the knurled grooves		perpendicular to the knurled grooves	
		50	250	50	250	50	250	50	250
bright-annealed	50	10%	–	7%	–	46%	–	24%	–
	250	–	–	–	–	–	23%	–	4%

Missing data in the table is either because no significant difference was observed or the comparison of peel resistance for different conditions was not applicable.

4.4 Conclusions

The effects of grinding and knurling of SSSS surface were investigated on peel resistance of adhesively bonded polymer adherends. By comparing the peel resistances from two modified surfaces with each other and with the as-received bright-annealed surface, the following conclusions were inferred.

The ground SSSS surface with $R_a < 1.00 \mu\text{m}$ enhanced the peel resistance of both adhesively bonded polymer adherends. The average increase in peel resistance was at least 6% for the case of HGF adherend at 50 mm/min peel speed. This is attributed to the increase in contact area and mechanical interlocking between the PSA and SSSS.

For ground SSSS surfaces, the normalized peel forces along and perpendicular to the grinding direction were similar. This likely stems from uniform spatial distribution of the microscale asperities on the ground SSSS surface.

For knurled surfaces which involved deeper and less frequent grooves, a decrease in peel resistance was observed for both adherend materials at low peel speed of 50 mm/min. This result is likely from the stress state complexity at the surface of the groove during peeling. Even increasing the peel speed could not fully recover the peel resistance of the LGF adherend to the level of bright annealed surface condition.

The effect of peeling direction with respect to the grooves geometry could not be neglected for knurled surfaces which involved grooves depths comparable to the adhesive thickness, as observed experimentally.

The increase in peel speed significantly increased the peel resistance of both adherends at all surface conditions by an increase in PSA peel resistance but also from increased plastic deformation of the adherends during peeling.

4.5 Acknowledgement

The authors are thankful for the financial support of this work by Natural Sciences and Engineering Research Council of Canada (NSERC), Ontario Centres of Excellence (OCE) and 3M Canada Corporation.

Chapter 5. Discussion

In this thesis, the interfacial adhesion of the polymer adherend in the PLSM structure has been assessed by using the 180° peel test. All of the peel test samples have been made by adhering two layers of the same adherend on the sheet metal substrate by means of an acrylic PSA. The second adherend layer has been used as an extra backing material during peeling to enhance the peel arm resistance to plastic or unstable deformation during peeling. The preliminary studies revealed that the two layers of adherends can suffice the need for prevention of unstable plastic deformation of all adherend types at all peel test conditions.

Three types of adherend materials, supplied by 3M Company (London, Ontario, Canada), have been used for PLSM manufacturing. In chapters 2 and 3, the adherends B and C which involved the same type of adhesive but different polymer films have been utilized. The polymer-metal interface properties for both of these two adherends could be assumed equal due to the fact that both of them involved the same type of adhesive. This assumption revealed the effect of type of polymer film on the interfacial adhesion properties of uniaxially deformed PLSMs. In chapter 4, two types of adherends namely HGF and LGF have been used for studying the effect of pre-existed surface roughness on the interfacial peel properties. The adherend LGF was identical to adherend type C which has been used in chapters 2 and 3. Both polymer film and adhesive type for adherends HGF and LGF were different, providing different types of interfaces and backing materials that could be used for different applications.

The 3M adherend materials were received as polymer films with pre-applied acrylic PSA on one side. At the stage of manufacturing of the adherends, the process-induced residual stress could be developed in these polymeric materials which consequently could affect their lamination and peel properties. These stresses, if existed, have not been considered in analysis of peel results. Rather than that, the effects of

difference in peel sample preparation have been considered extensively in this thesis. The objectives have been achieved either by alteration of the metallic substrate surface roughness before lamination, as described in chapter 2 and 4, or by uniaxial deformation of the PLSMs before peel test as presented in chapter 2.

Two new peel samples preparation protocols have been utilized in chapter 2. These protocols are based on pre-straining the PLSMs or the metallic substrate individually before lamination. The comparison between the results from these two types of peel samples has been attributed to the effect of deformation-induced residual stress on the interfacial peel properties. Increasing the tensile pre-strain values has increased the residual stress in the polymer adherends. However, the rate of increase has been dependent to the type of adherend material as well as the peel speed.

The analytical methodology in chapter 3 has revealed the significance of peel test speed on interface strength in cohesive zone modeling. The methodology is based on comparison between the peel force results at different speeds for two adherends B and C with identical adhesive type. The results have showed that a “reference peel speed” might exist at which the interface strength will be equal to the initial yield strength of peel arm for the studied materials. The results can potentially be implemented in future studies for development of rate-dependent cohesive zone models.

The effects of deformation-induced and pre-existed metallic substrate surface roughness on interfacial peel properties have been discussed in chapters 2 and 4 respectively. In chapter 2, the peeling of adherends B and C in PLSM samples which were prepared by lamination of the pre-strained substrate (PBL samples) resulted in almost constant peel force for all surface roughness conditions. In chapter 4, the metallic substrate surface roughness was altered with grinding and knurling processes before lamination. Ground surfaces enhanced the peel resistance of the adherends regardless of properties of PSAs and also direction of peeling. However, knurled surface with deep

and less frequent surface features deteriorated the peel resistance of adherends regardless of the type of the pressure sensitive adhesive. In general, two mechanisms have been considered for ramification of these observations. First, the increase in interfacial contact area between the adhesive and sheet metal substrate is considered as a reason for enhancing the adhesion properties. Second, the change in the stress state at the wall of the surface asperities decreases the peeling force required for interfacial de-bonding. In chapter 2 where the peel force was almost constant for the PBL samples with different surface roughness, it has been noted that none of these two above mechanisms were dominant during peeling of the studied adherend materials.

The metallic substrate surface roughness as described in chapters 2 and 4 could be distinguished in terms of difference in the range and texture of surface roughness. In chapter 2, the substrate surface roughness evolved with uniaxial deformation up to the $R_a = 0.40 \mu\text{m}$ at tensile pre-strain value of 0.20. In contrast, the ground surface in chapter 4 had the $R_a = 0.65 \mu\text{m}$ perpendicular to grinding direction. The average depth of the knurled groves in chapter 4 was $15 \mu\text{m}$. The ground and knurled surfaces had the oriented texture along the grinding and knurling directions (see Figure 4.2 and 4.3). However, the uniaxially deformed substrate had the uniform and non-oriented texture of asperities on the surface of the metallic substrate. Chapter 4 deals with substrate surface alteration before lamination by which neither the bulk of metallic substrate nor the polymer adherend will be deformed before or after lamination. This is in contrast with the objective in chapter 2 where the surface roughness evolution has been obtained by uniaxially deformation of substrate or PLSM.

In chapter 4, the univariate statistical analysis has been conducted for analyzing the effects of four variables of polymer adherend, surface condition, peel direction and speed on normalized peel force. For this purpose, the significance of difference in normalized peel force at various conditions was examined by using the t-test statistical analysis at confidence level of 95%. This method is capable to address the objective of

this study for assessment of the effect of metallic substrate surface alteration before lamination on peel properties. For future studies, it is also possible to perform the multivariate statistical analysis to assess the relationship between different variables and study how these variables work together to distinguish between different results at various peel test conditions.

Chapter 6. General conclusions

The assessment on interfacial adhesion in PLSMs is the core of this research study. Adhesion strength has been obtained for different testing conditions by using the 180° peel test.

A new experimental methodology has been proposed to decouple the effect of deformation-induced residual stress in polymer adherends from the effect of deformation-induced surface roughness of metallic substrate on interfacial adhesion properties of PLSMs. Results showed a decrease in peel strength by increasing the uniaxial tensile pre-strain value on PLSMs which have been deformed after lamination. In the presence of deformation-induced residual stress in polymer adherends, an increase in substrate surface roughness by increasing the pre-strain value cannot prevent the peel strength to decrease.

It has been shown that increasing the peel speed increases the peel strength for both types of PLSMs which have been pre-strained either before or after lamination. However, the rate of increase is different dependent to the type of the polymer adherend used in this study.

Cohesive zone modeling of the peel test results obtained from two types of PLSMs with the same adhesive and metallic substrate but with different polymer films indicates that there is likely a “reference peel speed” at which the interface strength, which is required for determining the adhesion fracture energy, could be equal to the yield strength of the peel arm. This evidence suggests that further research on rate-dependent cohesive zone models might offer the ability of reliable prediction of the interface strength.

Peel properties of the adherend from ground and knurled surfaces of the substrate at different peel speeds and in different peel directions with respect to the orientation of

the substrate surface features showed the dependency of the peel strength to the surface features as well as type of the polymer adherends and peel speeds. It has been found that grinding with sub-micron surface roughness promoted the adhesion strength in PLSMs while the knurled grooves with depth comparable to the adhesive thickness deteriorate the peel properties of the adherends from the altered substrate surface. In addition, comparison between two substrate surface conditions has shown that the peeling direction plays a statistically significant role on adhesion properties of the PLSMs involving the knurled metallic substrate surfaces with deeper and less frequent through-thickness grooves.

Recommendations for future work

- Finite element modeling of peel test on deformed PLSMs for assessment of the effect of plastic deformation on adhesion properties
- Research on rate-dependent cohesive zone modeling of peel test
- Verification of “reference peel speed” concept for the other types of interfacial bonded materials

Bibliography

- Adhesion, Adhesives and Composites Group, Imperial College, London, website: <http://www.me.imperial.ac.uk/AACgroup/index.html>, 2003.
- Aklonis, JJ; MacKnight, WJ, Introduction to Polymer Viscoelasticity, 2nd ed., John Wiley and Sons, New York, 1983.
- Azari, S; Papini, M; Spelt, JK, Effect of surface roughness on the performance of adhesive joints under static and cyclic loading. *Journal of Adhesion*, Vol. 86, 2010, pp. 742-764.
- Benedek, I., Pressure-sensitive adhesives and applications, 2nd ed., Marcel Dekker, Inc., New York, 2004.
- Carre, A; Schultz, J, Polymer-Aluminum Adhesion .1. The Surface-Energy of Aluminum in Relation to its Surface-Treatment, *Journal of Adhesion*, Vol. 15, Issue 2, 1983, pp. 151-161.
- Chan, EP; Ahn, D; Crosby, AJ, Adhesion of patterned reactive interfaces, *Journal of Adhesion*, Vol. 83, 2007, pp. 473-489.
- Chiche, A; Pareige, P; Creton, C, Role of surface roughness in controlling the adhesion of a soft adhesive on a hard surface, *Comptes Rendus de l' Academie des Sciences Serie IV*, 2000, pp. 1197-1204.
- Cho, TM; Choo, YS; Lee, MJ; Oha, HC; Lee, BC; Park, TH; Shin, YS, Effect of surface roughness on the adhesive strength of the heat-resistant adhesive RTV88, *Journal of Adhesion Science and Technology*, Vol. 23, 2009, pp. 1875-1882.
- Clyne, TW; Gill, SC, Residual stresses in thermal spray coatings and their effect on interfacial adhesion: a review of recent work, *Journal of Thermal Spray Technology*, Vol. 5, Issue 4, 1996, pp. 401-418.
- Comyn, J, *Adhesion Science*, Royal Society of Chemistry, Cambridge, UK, 1997.
- Dale, WC; Paster, MD; Haynes, JK, Mechanical-properties of acrylic pressure sensitive adhesives and their relationships to industry standard testing, *Journal of Adhesion*, Vol. 31, 1989, pp. 1-20.

- Fabrin, PA; Hoikkanen, AE; Vuorinen, JE, Adhesion of Thermoplastic Elastomer on Surface Treated Aluminum by Injection Molding, *Polymer Engineering and Science*, Vol. 47, Issue 8, 2007, pp. 1187-1191.
- Ge, J; Turunen, MPK; Kivilahti, JK, Surface Modification and Characterization of Photodefinable Epoxy/Copper Systems, *Thin Solid Films*, Vol. 440, Issue 1-2, 2003, pp. 198-207.
- Georgiou, I; Hadavinia, H; Ivankovic, A; Kinloch, AJ; Tropsa, V; Williams, JG; Cohesive Zone Models and the Plastically Deforming Peel Test, *Journal of Adhesion*, Vol. 79, Issue 3, 2003, pp. 239-265.
- Hadavinia, H; Kawashita, L; Kinloch, AJ; Moore, DR; Williams, JG, A numerical analysis of the elastic-plastic peel test, *Engineering Fracture Mechanics*, Vol. 73, 2006, pp. 2324-2335.
- He, MY; Evans, AG; Hutchinson, JW, Crack deflection at an interface between dissimilar elastic materials : role of residual stresses, *International Journal of Solids and Structures*, Vol. 31, No. 24, 1994, pp. 3443-3455.
- Huang, Y; Wang, J, Prediction of coating adhesion loss due to stretching, *International Journal of Adhesion and adhesives*, Vol. 40, 2013, pp. 49–55.
- Jensen, HM; Thouless, MD, Effects of residual-stresses in the blister test, *International Journal of Solids and Structures*, Vol. 30, 1993, pp. 779-795.
- Kawashita, LF; Moore, DR; Williams, JG, Comparison of Peel Tests for Metal-Polymer Laminates for Aerospace Applications, *Journal of Adhesion*, Vol. 81, Issue 6, 2005, pp. 561-586.
- Kim, KS; Aravas, N, Elastoplastic Analysis of the Peel Test, *International Journal of Solids and Structures*, Vol. 24, Issue 4, 1988, pp. 417-735.
- Kim KS; Kim J, Elasto-Plastic Analysis of the Peel Test for Thin-Film Adhesion, *Journal of Engineering Materials and Technology-Transactions of The ASME*, Vol. 110, Issue 3, 1988, pp. 266-273.
- Kim, SH; Na, SW; Lee, NE; Nam, YW; Kim, YH, Effect of Surface Roughness on the Adhesion Properties of Cu/Cr Films on Polyimide Substrate Treated by Inductively Coupled Oxygen Plasma, *Surface & Coatings Technology*, Vol. 200, Issue 7, 2005, pp. 2072-2079.

- Kinloch, AJ; Lau, CC; Williams, JG, The Peeling of Flexible Laminates, *International Journal of Fracture*, Vol. 66, Issue 1, 1994, pp. 45-70.
- Kinloch, AJ; Williams, JG, The Mechanics of Peel Test, *The Mechanics of Adhesion*, Edited by Dillard, DA; Pocius, AV, Elsevier, Amsterdam, NL, 2002.
- Krishna, A, Edge Delamination of Residually Stressed Thin Films: Viscoelastic Effects, *International Journal of Fracture*, Vol. 75, 1996, pp. 215-228.
- Lacombe R, *Adhesion Measurement Methods: Theory and Practice*, Taylor & Francis, New York, US, 2005.
- Lee, HY; Qu, JM, Microstructure, Adhesion Strength and Failure Path at a Polymer-Roughened Metal Interface, *Journal of Adhesion Science and Technology*, Vol. 17, Issue 2, 2003, pp. 195-215.
- Marshall, SJ; Bayne, SC; Baier, R; Tomsia, AP; Marshall, GW, A Review of Adhesion Science, *Dental Materials*, Vol. 26, Issue 6, 2010, pp. e11-e16.
- Moore, DR, An Introduction to the Special Issue on Peel Testing, *International Journal of Adhesion & Adhesives*, Vol. 28, 2008, pp. 153–157.
- Moore, DR; Williams, JG, Peel Testing of Flexible Laminates, *Fracture Mechanics Testing Methods for Polymers, Adhesives and Composites*, Edited by Moore, DR; Pavan, A; Williams, JG, Elsevier, Oxford, UK, 2001.
- Müller, WD; Seliger, K; Meyer, J; Gilbert, JL, The Improvement of Adhesion of Polymer on Titanium Surface After Treatment With TEA-CO₂ Laser Irradiation, *Journal of Materials Science-Materials in Medicine*, Vol. 5, Issue 9-10, 1994, pp. 692-694.
- (a) Noori, H; Jain, M; Nielsen, K; Brandys, F, Influence of metallic substrate surface engineering on peel resistance of adhesively bonded polymer film, *Journal of Adhesion Science and Technology*, Vol. 29, No. 13, 2015, pp. 1403-1413.
- (b) Noori, H; Jain, M; Nielsen, K; Brandys, F, Significance of peel test speed on interface strength in cohesive zone modeling, *Journal of Adhesion*, Accepted for publication, doi: 10.1080/00218464.2014.993755.
- Persson, BNJ; Tosatti, E, The effect of surface roughness on the adhesion of elastic solids, *Journal of Chemical Physics*, Vol. 115, 2001, pp. 5597-5610.

- Rahulkumar, P; Jagota, A; Bennison, SJ; Saigal, S, Cohesive element modeling of viscoelastic fracture: application to peel testing of polymers, *International Journal of Solids and Structures*, Vol. 37, 2000, pp. 1873-1897.
- Ranucci, E; Sandgren, A; Andronova, N; Albertsson, AC, Improved Polyimide/Metal Adhesion by Chemical Modification Approaches, *Journal of Applied Polymer Science*, Vol. 82, Issue 8, 2001, Pp. 1971-1985.
- Rincon Troconis, BC; Frankel, GS, Effect of roughness and surface topography on adhesion of PVB to AA2024-T3 using the blister test, *Surface & Coatings Technology*, Vol. 236, 2013, pp. 531-539.
- Sancaktar, E; Ma, W, Mathematical assessment of the effects of parabolic and spherical surface topographies on the interfacial state of stress, *Journal of Adhesion*, Vol. 85, 2009, pp. 302-323.
- Schultz, J; Nardin M, *Theories and Mechanisms of Adhesion, Adhesion Promotion Techniques*, Edited by Mittal, KL; Enstib, AP, Marcel Dekker, Inc, New York, US, 1999.
- Takiguchi, M; Yoshida, F, Deformation characteristics and delamination strength of adhesively bonded aluminum alloy sheet under plastic bending, *JSME International Journal Series A-Mechanics and Material Engineering*, Vol. 46, 2003, pp. 68–75.
- Takiguchi, M; Yoshida, F, Effect of forming speed on plastic bending of adhesively bonded sheet metals, *JSME International Journal Series A-Mechanics and Material Engineering*, Vol. 47, 2004, pp. 47–53.
- Teixeira, FG; da Silva, LFM, Study of influence of substrate topography on stress distribution in structural adhesive joints, *Journal of Adhesion*, Vol. 87, 2011, pp. 671–687.
- Thouless, MD; Jensen, HM, Elastic Fracture-Mechanics of the Peel-Test Geometry, *Journal of Adhesion*, Vol. 38, Issue 3-4, 1992, pp. 185-197.
- Thouless, MD; Jensen, Hm, The effect of residual-stresses on adhesion measurements, *Journal of Adhesion Science and Technology*, Vol. 8, 1994, pp. 579-586.
- van den Bosch, MJ; Schreurs, PJG; Geers, MGD; van Maris, MPFHL, Interfacial characterization of pre-strained polymer coated steel by a numerical–experimental approach, *Mechanics of Materials*, Vol. 40, 2008, pp. 302–317.

- van Tijum, R; Vellinga, WP; De Hosson, JThM, Adhesion along metal-polymer interfaces during plastic deformation, *Journal of Materials Science*, Vol 42, 2007, pp. 3529-3536.
- Vayeda, R; Wang, J, Adhesion of coatings to sheet metal under plastic deformation, *International Journal of Adhesion and Adhesives*, Vol. 27, 2007, pp. 480-492.
- Vellinga, WP; Fedorov, A; De Hosson, JT, Residual stress pinning of delamination fronts on polymer-metal interfaces, *Thin Solid Films*. Vol. 517, 2008, pp. 841-847.
- Watts, JF; Castle, JE, The Application of X-Ray Photoelectron-Spectroscopy to the Study of Polymer-to-Metal Adhesion .2. The Cathodic Disbondment of Epoxy Coated Mild-Steel, *Journal of Materials Science*, Vol. 19, Issue 7, 1984, pp. 2259-2272.
- Wei, Y; Hutchinson, JW, Interface Strength, Work of Adhesion and Plasticity in the Peel Test, *International Journal of Fracture*, Vol. 93, Issue 1-4, 1998, pp. 315-333.
- Williams, JG, Energy release rates for the peeling of flexible membranes and the analysis of blister tests, *International Journal of Fracture*, Vol. 87, 1997, pp. 265-288.
- Williams, JG; Hadavinia H, Analytical solutions for cohesive zone models, *Journal of the Mechanics and Physics of Solids*, Vol. 50, 2002, pp. 809-825.
- Wu, PK; Lu, TM; Metal/Polymer Adhesion Enhancement by Reactive Ion Assisted Interface Bonding and Mixing, *Applied Physics Letters*, Vol. 71, Issue 18, 1997, pp. 2710-2712.
- Yu, H; Hutchinson, JW, Delamination of thin film strips, *Thin Solid Films*, Vol. 423, 2003, pp. 54-63.